

**Manuscript Title:**

**MODAL PUSHOVER AND RESPONSE HISTORY ANALYSES OF A  
MASONRY CHIMNEY BEFORE AND AFTER SHORTENING**

**Authors:**

**Fabio Minghini** (Corresponding author)

Engineering Department – University of Ferrara

Via Saragat 1, 44122 Ferrara – Italy

Phone: +39 (0)532 974912

Fax: +39 (0)532 974870

E-mail: [fabio.minghini@unife.it](mailto:fabio.minghini@unife.it)

**Elisa Bertolesi**

Department of Structural Engineering – Polytechnic Institute of Milan

Piazza Leonardo da Vinci 32, 20133 Milan – Italy

E-mail: [elisa.bertolesi@polimi.it](mailto:elisa.bertolesi@polimi.it)

**Antonio Del Grosso**

Engineering Department – University of Ferrara

Via Saragat 1, 44122 Ferrara – Italy

Phone: +39 (0)532 974929

Fax: +39 (0)532 974870

E-mail: [antonio.delgrosso@student.unife.it](mailto:antonio.delgrosso@student.unife.it)

**Gabriele Milani**

Department of Structural Engineering – Polytechnic Institute of Milan

Piazza Leonardo da Vinci 32, 20133 Milan – Italy

Phone: +39 (0)2 2399 4290

Fax: +39 (0)2 2399 4220

E-mail: [milani@stru.polimi.it](mailto:milani@stru.polimi.it)

**Antonio Tralli**

Engineering Department – University of Ferrara

Via Saragat 1, 44122 Ferrara – Italy

Phone: +39 (0)532 974822

Fax: +39 (0)532 974870

E-mail: [antonio.tralli@unife.it](mailto:antonio.tralli@unife.it)

# **Modal pushover and response history analyses of a masonry chimney before and after shortening**

Fabio Minghini<sup>a</sup>, Elisa Bertolesi<sup>b</sup>, Antonio Del Grosso<sup>a</sup>, Gabriele Milani<sup>b</sup>,  
and Antonio Tralli<sup>a</sup>

<sup>a</sup> *Engineering Department, University of Ferrara, Ferrara, Italy*

<sup>b</sup> *Polytechnic Institute of Milan, Milan, Italy*

## **ABSTRACT**

The 50 m high masonry chimney located in the old industrial facility that houses the School of Engineering of the University of Ferrara, Italy, suffered severe damages during the 2012 Emilia seismic sequence. Afterward, for security reasons, the upper damaged 12.40 m were disassembled. Both before and after shortening, the ratio between the effective mass of the fundamental mode and the total mass is approximately 20%, leading standard pushover analysis methods not to be appropriate for estimating the seismic demand. Using a single, consistent 3D FE formulation, the results of a Modal Pushover Analysis (MPA) and four nonlinear Response History Analyses (RHA) for the shortened and the original chimney were presented in the paper. The ground motions considered in the simulations are accelerograms recorded during recent and less recent devastating seismic events in Italy, New Zealand, and Japan.

For both chimneys, a very good agreement between MPA and RHA was observed in terms of lateral displacements. Moreover, for the 50 m high chimney, a strong similarity was observed between the damage maps deriving from the MPA and those obtained with the RHA. All analyses confirmed a significant contribution of the higher modes. For the shortened chimney, the MPA revealed damages in the lower part of the stack (8–21 m), because of a prevailing influence of the

fundamental mode. In the RHA, a more evident contribution of the higher modes was observed, probably because of the effect of the vertical component of the ground motion, not accounted for in the MPA.

**Keywords:** Masonry chimney; Modal pushover analysis; Nonlinear response history analysis; Higher modes

## 1. Introduction

The seismic analysis of unreinforced masonry chimneys and towers represents a real challenge for the Earthquake Engineering, especially because of the difficulties in developing predictive computational models for reproducing the nonlinear masonry response in the dynamic field. The problem complexity is often increased by the strong influence of the higher modes of vibration. One of the first studies on the possible failure mechanisms of masonry chimneys under earthquake excitation is reported in [1], where an attempt to explain earthquake-induced damages observed in some chimneys in California and China in the Eighties was presented. In [2], based on a simplified model using elastic beam elements connected through nonlinear joints, and accounting for the soil-structure interaction, a seismic vulnerability assessment for a 97.2 m high masonry tower in the historical centre of Bologna, Italy, was presented. More recently, an increased computing power allowed for more advanced analyses using two- or three-dimensional finite elements. In [3]–[4], typical first-mode failure mechanisms, with collapse being triggered by masonry cracking at the chimney base, were described. In [5], an experimentally-calibrated numerical model is used to verify the effectiveness of the seismic strengthening of an industrial masonry chimney using CFRP strips. A 70 m high stone masonry minaret was analyzed in [6], where a critical comparison between nonlinear static and dynamic analysis methods was reported. In particular, in that work it was concluded that the pushover analysis is not able to reproduce the change in the dynamic properties of the structure typically occurring during severe ground motions, leading to

unacceptable underestimations of lateral displacements and drifts. An interesting state-of-the-art review of seismic assessment and strengthening techniques of masonry chimneys is reported in [7]. The effects of wind and seismic actions on a damaged chimney in Alicante, Spain, were analyzed in a recent work [8] through a numerical model that includes the longitudinal cracks observed along the stack. With regard to the in-situ characterization of masonry chimneys, an experimentally-based model updating technique was developed in [9]. The procedure proposed can detect the stiffness variations along the chimney stack due to possible damages, resulting to be a useful tool for assessing the structural stability [10].

In the present paper, a seismic damage assessment for an unreinforced masonry chimney built at the beginning of the 20th century in the service of a sugar factory in Ferrara, Italy, is presented. The chimney is no longer in use since the end of the Fifties, when electric power replaced steam in the industry, but represents a symbol in the industrial history of the Po River Plain and is protected by the Italian Ministry of Cultural Heritage. In the aftermath of the 2012 earthquake sequence in Northern Italy (Emilia earthquake), a survey campaign put in evidence diagonal cracks in the outer surface of the stack at an altitude of approximately 40-45 m. Preliminary numerical analyses in both linear and nonlinear field highlighted the role played by the higher modes of vibration in determining the damages [11]. The behavior factor estimated on the basis of a Modal Pushover Analysis (MPA) was in line with the value  $q = 1.5$  recommended by [12], indicating a very low dissipative capacity. In the same work, a number of nonlinear Response History Analyses (RHA) were conducted using a numerical model with two-dimensional rigid finite elements connected through nonlinear interfaces, that allowed for partially explaining the vulnerability of the upper part of the stack.

The geology of the Po River Plain is characterized by very deep alluvial deposits. This feature, although the distances of the chimney from the epicenters of the two mainshocks exceed 30 km, might have likely amplified the seismic shake, contributing to the damages. Anyway, the observed damage pattern was associated with a significant mortar deterioration in the same part of the

structure (i.e., at elevation  $z = 38$  to  $50$  m), that certainly weakened the stack and probably triggered the crack propagation. This situation, because of the proximity of the chimney to buildings containing university classrooms and offices, suggested, for security reasons, a shortening of approximately  $12$  m to remove the damaged part. The current chimney (Figure 1a) is  $37.6$  m high, and is not substantially damaged. In view of a possible reassembling of the removed part to recover the original,  $50$  m high configuration (Figure 1b), the principal objective of the present investigation is to compare the seismic response of the shortened chimney with that of the original structure. With this aim, MPA and RHA of the two structures were carried out using a single consistent numerical formulation with three-dimensional nonlinear finite elements. Because the effective mass associated with the fundamental mode of vibration is only approximately  $20\%$  of the total mass for both the  $37.6$  m and the  $50$  m high chimney, it was necessary to include in the MPA four and five “modal” force distributions, respectively. In these analyses, the target displacements were computed from the inelastic response spectrum, i.e., the response spectrum evaluated for elasto-plastic systems, of the ground motion recorded the May 29<sup>th</sup>, 2012, by the seismic station in Mirandola, at an epicentral distance of approximately  $5$  km. In the RHA, both horizontal and vertical components of the same, and of other three real ground motions were alternatively applied at the base of the two chimneys. Described and comparatively discussed in the paper are lateral displacement profiles and damage maps obtained for the chimneys from the static and dynamic analysis methods.

## **2. Numerical models**

### **2.1. Geometry of the chimneys**

The geometry of the original,  $50$  m high chimney resulting from a preliminary inspection was first reported in [11]. Afterward, an accurate survey with 3D laser scanner technique allowed for an overall geometry update. The resulting new values of the outer diameter and the corresponding thicknesses are reported in Table 1 for ten cross sections. Note that section S7, located at  $z = 37.6$  m, corresponds to the top of the shortened chimney. The analyses of the shortened chimney

reported hereinafter assumed an initially undamaged state, because earthquake-induced damages were observed only in the removed part of the stack. Moreover, in view of a possible reassembling of this part in the near future, also the 50 m high chimney was assumed to be initially undamaged.

## **2.2. FE discretization**

For the numerical analyses, FE models using 8-node solid (brick) elements were developed. In particular, for the shortened chimney, 75 and 16 equal subdivisions along the vertical axis and in the planes of the cross sections, respectively, were used, resulting in a total of 1200 finite elements and 2432 nodes. The choice of this FE discretization, presenting one single subdivision through the thickness, was motivated by the need for enabling accurate numerical solutions while limiting the computational effort. A second, refined FE mesh was implemented using two subdivisions through the thickness, leading to 2400 finite elements and 3648 nodes. The comparison between the two numerical models with regard to the frequency and pushover analyses is presented in the next Section. Herein we can state in advance that the coarser numerical model proved to be sufficiently accurate. Therefore, using the same meshing criterion, the original, 50 m high chimney was discretized using 100 and 16 equal subdivisions along the vertical axis and in the planes of the cross sections, respectively, resulting in 1600 solid elements and 3232 nodes.

The influence of the soil-structure interaction on the seismic response of slender structures such as chimneys and towers may be relevant [13], and a suitable analysis of this phenomenon should be based on extensive in-situ investigations [14]. In particular, in [15] and [16] the dynamic characterization of Medieval brickwork bell towers was presented. In that works, masonry properties such as Young's and transverse shear elastic moduli  $E$  and  $G$ , as well as shear wave velocity  $V_s$  in the surrounding soil, were identified by minimizing a cost function depending on experimentally determined natural frequencies and corresponding numerical estimates. To excite the towers, impulsive loading was used. In the FE models developed, the soil-structure interaction was accounted for by defining, at the tower base, suitable translational and rotational spring

stiffnesses that were related to the estimated  $V_s$  according to the formulation presented in [17]. Very recently, dynamic identification analysis and model updating of the Ghirlandina tower in Modena, Italy, were published [18]. Mode shapes and corresponding vibration frequencies and damping ratios were obtained using ambient excitation. Some vibration mode was found particularly sensitive to the soil deformability.

It is worth observing that the towers studied in [15] and [18] have a relatively complex geometry and present a structural connection with the adjacent church, that certainly gives rise to a global stiffening effect. This undoubtedly justifies an accurate assessment of the dynamic behavior.

For the 50 m high chimney investigated in the present paper, no dynamic characterization was carried out until shortening occurred in 2012, above all because the structure was no longer in use since the Fifties. Nevertheless, for the shortened chimney a series of dynamic tests has already been planned for the near future, together with an accurate calibration of soil-structure interaction parameters. Actually, through a simplified numerical model with beam elements, the study presented in [11] showed that, for the 50 m high chimney, the soil-structure interaction has a negligible effect on vibration frequencies and mode shapes, at least from a technical point of view. In fact, by adopting typical soil properties for the specific site and dynamic stiffnesses in accordance with Pais and Kausel's formulation [17], for the five mode shapes used for the MPA (see Section 3) the difference in terms of natural frequencies with respect to the fixed-base case lies in the range 0.3%–4.2%, with lower and upper bounds corresponding to the fundamental and the sixth mode, respectively. Because of the frequency dependence of the dynamic impedances at the chimney base, weighted mean values of these stiffness parameters, obtained using the effective modal masses as the weights, were adopted in [11]. With regard to the four modes of the shortened chimney used for the MPA, analogous calculations would yield to differences with respect to the chimney on fixed base between 0.6% (fundamental mode) and 5.4% (fifth mode).

Therefore, although an experimental proof of these preliminary results is certainly needed, the two chimneys analyzed in the present paper were assumed to rest on a fixed base.



### 2.3. Constitutive relationships for masonry

The definition of suitable constitutive relationships for masonry is still an open problem, especially in the dynamic field. In this paper, software packages DIANA [19] and ABAQUS [20] were used to perform pushover and response history analyses, respectively. With regard to the first program, the material nonlinearities were reproduced by means of a traditional total strain crack model, belonging to the family of the smeared crack constitutive laws [21]. It is worth noticing that inhomogeneity of masonry is not accounted for in this model, that assumes an isotropic material behavior both in the elastic field and at collapse. However, the use of this model for reproducing the nonlinear behavior of masonry may be adequate if combined with proper engineering reasoning. In particular, this approach was shown to be justified [3], [22]–[23] provided that the model parameters are adapted to fit a response averaged between vertical and horizontal compression. In the present paper, the effects due to cracking were taken into account by using a linear softening for the stress-strain relationship in tension and a constant shear retention factor  $\beta = 0.05$ . Because of the assumed isotropy of the mechanical behavior, the tension damage would affect at the same extent the shear behavior, making masonry incapable of preserving a shear stress transfer along the cracks. To overcome this drawback, a shear retention factor [21], [24] is usually introduced. After cracking, the role of  $\beta$  (Figure 2) is to ensure a residual shear transfer capacity along the crack due to friction. The model parameters are summarized in Table 2. In particular, the compressive strength was estimated from the mean compressive strength obtained from laboratory tests [11] divided by a confidence factor  $CF = 1.2$ , suitable for a knowledge level KL2 according to [25], whereas, in the absence of a specific experimental characterization, the value of Young's modulus was chosen in agreement with the indications reported in [26] for existing masonry structures.

The constitutive model used for the numerical simulations in ABAQUS, the so called Concrete Damage Plasticity (CDP) model [27], substantially represents the extension to the cyclic case of the previously described model. It is based on the assumption of a scalar isotropic damage with distinct

damage parameters in tension and in compression and is particularly suitable for applications in which the material exhibits damage, especially under loading-unloading conditions, and therefore for dynamic analyses. A different inelastic behavior in tension and in compression was then introduced, as shown in Figure 3. To describe the multi-dimensional behavior in the inelastic range, masonry was assumed to obey a Drucker-Prager strength criterion with non-associated flow rule. A parameter  $K_c = 2/3$ , applied to the analytical expression for the Drucker-Prager surface in the principal stress space, allowed distorting the surface, making them more similar to that of the Mohr-Coulomb criterion (Figure 4). Physically, parameter  $K_c$  is interpreted as the ratio of the distance, measured on the deviatoric cross section of the failure surface, between the hydrostatic axis and the tension meridian (T.M. in Figure 4) to the distance, evaluated on the same cross section, between the hydrostatic axis and the compression meridian (C.M. in Figure 4). This ratio is always larger than 0.5, and when it assumes the value of 1, the deviatoric cross section of the failure surface becomes a circle (as in the classical Drucker-Prager strength domain). Majewski, in [28], reported that, according to experimental results, this value amounts to 0.6 for a mean normal stress equal to zero, and slowly increases with the mean compressive stress. The CDP model recommends to assume  $K_c = 2/3$ . The resulting strength domain is similar to that formulated by William and Warnke [29] using a combination of three mutually tangent ellipses.

A value of  $10^\circ$  was adopted for the dilatation angle, which seems reasonable for masonry subjected to a moderate-to-low level of vertical compression. This value is in agreement with experimental evidences available in the literature [30]. To avoid numerical convergence issues, the tip of the conical Drucker-Prager strength domain was smoothed using a hyperbola. Software ABAQUS allows for smoothing the strength domain by means of an eccentricity parameter, which in the  $q$ - $p$  plane represents the distance between the points of intersection with the  $p$ -axis of the cone and the hyperbola (Figure 5). A value of 0.1 was adopted in the simulations for this parameter. The available experimental results on regular masonry wallettes show a moderate orthotropy ratio (around 1.2) under biaxial stress states in the compression-compression region [31]. A suitable

model should also take into account the ratio between the ultimate compressive strength in a biaxial stress state and that in uniaxial conditions. This ratio, typically taking similar values for concrete and masonry, was set equal to 1.16 [32]. The final stress-strain relationship in tension adopted for the dynamic analyses (Figure 3a) follows a linear-elastic branch up to the peak stress  $f_t = 0.1$  MPa. Then, micro-cracks start to propagate within the material leading to a macroscopic softening. In compression (Figure 3b), the response is linear up to the yield stress  $f_{c0} = 3$  MPa. Then, a linear hardening was assumed up to the crushing stress  $f_{cu} = 3.5$  MPa, followed by a linear softening branch. The damage variables in tension (index “t”) and compression (index “c”) are defined by means of the following standard relations:

$$f_t = E_0(1 - d_t)(\varepsilon_t - \varepsilon_t^{pl}) \quad (1)$$

$$f_c = E_0(1 - d_c)(\varepsilon_c - \varepsilon_c^{pl}) \quad (2)$$

where  $f_t, f_c$  = uniaxial stresses;  $E_0$  = initial elastic modulus;  $\varepsilon_t, \varepsilon_c$  = uniaxial total strains;  $\varepsilon_t^{pl}, \varepsilon_c^{pl}$  = equivalent plastic strains; and, finally,  $d_t, d_c$  = damage parameters. In the present study, only tension damage was assumed to be active, because the adopted tensile strength of the material is significantly lower than the compressive strength. In other words, when the tensile strain attains the critical value of 0.1 MPa (Table 2), the material starts to degrade showing, in the unloading phase, a modulus  $E < E_0$ .

Preliminary numerical tests on prismatic solids showed that the constitutive models provided by the two software packages are substantially equivalent for the monotonic load case.

Geometric nonlinearities were accounted for in all analyses. The masonry mass density assumed in the simulations is  $w = 1800$  kg/m<sup>3</sup> [11], resulting in a total mass of 542380 kg and 589000 kg for the shortened and the original chimney, respectively.

### 3. Modal pushover analysis

In the present paper, the Modal Pushover Analysis (MPA) was used to assess the seismic damage to be expected in the shortened chimney, and to provide a comparison with the earthquake response of the original structure.

#### 3.1. Modal pushover analysis procedure

The MPA was introduced in [33] for multistorey framed structures to improve the pushover methods based on force distributions proportional to one single mode of vibration. The basic idea of the MPA method is to combine the results of  $N$  pushover analyses, the  $n$ -th of which is based on the invariant force distribution proportional to  $\mathbf{s}_n^* = \mathbf{M}\boldsymbol{\phi}_n$ , with  $\mathbf{M}$  and  $\boldsymbol{\phi}_n$  being global mass matrix and  $n$ -th elastic mode shape, respectively. The choice of number  $N$  should obviously be governed by the amount of activated mass. In the  $n$ -th analysis, the structure is pushed to the top displacement

$$u_{in0} = \Gamma_n \phi_{in} D_n \quad (3)$$

where  $\Gamma_n$  is the modal participation factor defined by the following relation [34]

$$\Gamma_n = L_n / M_n \quad (4)$$

and  $\phi_{in}$  and  $D_n$  represent the component of eigenvector  $\boldsymbol{\phi}_n$  corresponding to the monitored node on the top of the structure and the peak response for the  $n$ -th mode SDOF system, respectively.

Quantities  $L_n$  and  $M_n$  appearing in Eq. (4) may be written in the form [34]:

$$L_n = \boldsymbol{\phi}_n^T \mathbf{M} \boldsymbol{\iota} \quad (5)$$

$$M_n = \boldsymbol{\phi}_n^T \mathbf{M} \boldsymbol{\phi}_n \quad (6)$$

where  $\boldsymbol{\iota}$  is the influence vector.

Each of the  $N$  modal pushover curves is idealized as a bilinear force-deformation relation, and the corresponding peak deformation is used to determine the target value of the top displacement. In particular, displacement  $D_n$  to be used in Eq. (3) may be obtained from the inelastic response spectrum. Alternatively, indicating with  $\mu_n = D_{nu}/D_{ny}$  the ductility factor, i.e., the ratio between

ultimate and yielding responses of the  $n$ -th mode SDOF system, and with  $R_n = A_n/A_{ny}$  the  $n$ -th strength reduction factor, with  $A_{ny}$  and  $A_n$  being the maximum pseudo-accelerations for the inelastic and the equivalent elastic systems, respectively, the peak response  $D_n$  may be written as [34]:

$$D_n = (\mu_n/R_n)(T_n^*/2\pi)^2 A_n \quad (7)$$

In Eq. (7),  $T_n^* = 2\pi\sqrt{L_n/k_n^*}$  is the elastic period of vibration of the  $n$ -th inelastic system, whereas  $k_n^*$  indicates its elastic stiffness. In the framework of the MPA, the peak modal responses (i.e., displacements, strains, stresses, internal forces, stresses, etcetera) are combined according to the Square-Root-of-Sum-of-Squares (SRSS) or the Complete Quadratic Combination (CQC) rules [33] traditionally used in the modal response spectrum analysis.

In [33], the MPA procedure was obtained by simply reformulating the standard response spectrum method. Therefore, for elastic buildings modal pushover and response spectrum analyses are completely equivalent. The basic difference between these two procedures relies upon the fact that the response spectrum analysis is restricted to the linear elastic field, whereas the MPA takes account of the material nonlinearities, and is then suitable for the damage assessment. Although the superposition of uncoupled modal responses has no physical meaning in the case of MDOF inelastic systems, the MPA procedure was shown to perform significantly better than traditional pushover procedures in evaluating story drifts, plastic hinge rotations [35] and member forces [36] for framed structures. Moreover, for these structures, the MPA procedure was shown to be able to reproduce the plastic mechanisms due to the higher-mode effects [37]–[38]. These works pointed out that the seismic demands associated with the higher modes may generally be evaluated assuming that the building remains elastic. The effectiveness of the MPA method in capturing the behavior of tall and unsymmetric-plan buildings was then investigated in [39] and [40], respectively, including two components of the ground motion. In both cases, encouraging results were obtained. Finally, applications of the MPA to the selection and scaling of ground motion records for use in nonlinear RHA were developed by searching for the best fit between the

deformation of the first-mode inelastic SDOF system evaluated from the first mode pushover curve of the building and that produced by the scaled record [41]–[42]. Very recently this scaling procedure, generally referred to as Modal Pushover-based Scaling (MPS), was extended to unsymmetric-plan buildings [43], confirming a better performance in comparison with the procedure provided by the American standard. The use of the MPA method for the seismic assessment of high-rise cantilevers made of no-tension materials could appear, at a first sight, to be straightforward in many cases. However, in the case of the Qutb Minar in Delhi (India), a 70 m high three-leaf masonry minaret, the MPA was not able to capture the change of the dynamic behavior occurring during the seismic event [6], leading to underestimations of the roof lateral displacements in comparison with the nonlinear RHA. Conversely, with regard to the 50 m high masonry chimney investigated in [11], the MPA was proved to be effective in detecting the actual damage pattern caused by the 2012 Emilia, Italy, earthquake sequence. Therefore, in the present investigation the MPA procedure was used again for a new (because of the recent geometry update) full 3D seismic analysis of the 50 m high chimney, and for that of the shortened, 37.6 m high chimney. The analyses presented in the following focus on vibration mode shapes and seismic behavior of the two chimneys. In particular, the “modal” pushover curves and the relevant damage patterns for the two structures are discussed and compared.

### 3.2. Vibration frequencies and mode shapes

In the following, the vibration modes will be referred to as “ $mn$ ” for the 37.6 m high chimney and “ $Mn$ ” for the 50 m high chimney, where  $n$  indicates the generic mode number. The vibration frequencies and periods corresponding to the six most significant mode shapes are reported in Table 3 and Table 4 for the shortened and the original chimney, respectively. The corresponding mode shapes are shown in Figures 6 and 7. Also reported in the tables are the modal participation factors  $\Gamma_n$  and the effective modal masses  $M_n^*$ , that result from the following expression [34]:

$$M_n^* = L_n \Gamma_n = L_n^2 / M_n \quad (8)$$

where  $\Gamma_n$ ,  $L_n$  and  $M_n$  are obtained from Eqs. (4)–(6). With regard to the 50 m high chimney, the small differences with respect to the frequencies reported in [11] are to be ascribed to the recent geometry update. It can be noted that five and six modes are needed for the shortened and the original chimney, respectively, to activate a mass larger than 75% of the total mass. The most important modes in terms of effective modal mass are m3 ( $f_3 = 8.07$  Hz and  $M_3^*/M = 23.8\%$  in Table 3) and M1 ( $f_1 = 0.46$  Hz and  $M_1^*/M = 20.6\%$  in Table 4).

In order to verify the accuracy of the obtained results, the frequency analysis of the 37.6 m high chimney was repeated using the refined FE model with two subdivisions through the thickness. The percent differences in terms of frequency and effective modal mass with respect to the coarser FE discretization resulted to be negligible (see Table 5).

### 3.3. Analysis of the shortened chimney

All modes with effective mass larger than 5.5% of the total mass were used for the MPA of the shortened chimney. Therefore, lateral force profiles  $\mathbf{s}_n^*$ , with  $n$  alternatively taking the values 1, 2, 3, and 5, were used, corresponding to the first four modes reported in Table 3. The amount of activated mass for these modes is approximately 71% of the total mass.

To reproduce the lateral load profiles  $\mathbf{s}_n^* = \mathbf{M}\boldsymbol{\phi}_n$ , the mass was assumed to be lumped at the centroids of the 75 annular-section segments representing the model subdivisions along the  $z$ -axis (see Sect. 2.2), and also vector  $\boldsymbol{\phi}_n$  was referred to the same points. Then, each of the 75 resulting forces was uniformly distributed on the 16 solid elements of the corresponding chimney segment in the form of 16 equal body forces applied to the element centroids.

The nondimensional lateral forces, normalized to the maximum value, are reported in Figure 8a versus the elevation ( $z$ ). The corresponding plots of the total base shear versus the horizontal displacement of one of the nodes located at  $z = 37.6$  m are reported in Figure 9a, where open and solid circle data points refer to target displacements  $u_{m0}$  evaluated using Eq. (3). In particular, the peak displacement of the  $n$ -th mode inelastic SDOF system, i.e.,  $D_n$  in Eq. (3), was determined by a

nonlinear Response History Analysis (RHA) using the horizontal (East-West) acceleration component of the May 29<sup>th</sup>, 2012, ground motion recorded in Emilia, Italy, in proximity of the epicentre, and conveniently scaled to obtain compatibility with the elastic spectrum provided by the Italian Building Code [26] (ER ground motion, last row of Table 6). Equivalently, Eq. (7), or the inelastic response spectrum for the  $n$ -th SDOF system may be used to determine  $D_n$ .

In order to estimate the possible damage evolution of the chimney undergoing seismic excitations of increasing intensity, target displacements  $u_{m0}$  were evaluated for two different ground motion scale factors ( $SF_{ER}$ ), i.e.,  $SF_{ER} = 1$  (open circle data points in Figure 9a), and  $SF_{ER} = 3$  (solid circle data points in Figure 9a). It can be noted by inspection that, for  $SF_{ER} = 1$ , only the target point for mode m1 turns out to be located on the “plastic” branch of the corresponding pushover curve, whereas no damage is to be expected for the other modes. Then, the actual damage pattern of the chimney is expected to be mainly influenced by the fundamental mode. The total base shear estimated by combining the four modal contributions with the SRSS rule is 754 kN, approximately corresponding to 14% of the self weight. For  $SF_{ER} = 3$ , all seismic demands give a significant contribution to the damage pattern of the chimney.

The peak displacements ( $D_n$ ) evaluated for the modes responsible for the damages, i.e., m1 for  $SF_{ER} = 1$ , and m1, m2, m3, and m5 for  $SF_{ER} = 3$ , are compared in Figure 10a with the displacement spectra for the East-West component of ER earthquake. In particular, open and solid circle data points in Figure 10a refer to  $SF_{ER} = 1$  and 3, respectively. It is worth noting that, for the fundamental mode ( $T_1 = 1.18$  s, see Table 3), the values of  $D_1$  are quite close to the corresponding spectral displacements, confirming that, for relatively large periods, the peak displacement for an inelastic system is well approximated by that of an elastic system of equal period [34].

The lateral displacement profile obtained from the MPA for  $SF_{ER} = 1$  is reported in Figure 9c (red solid line). This profile was computed by combining, for each cross section, the values of the lateral displacement corresponding to the four target top displacements using the SRSS rule. The maximum lateral displacement attained at the top resulted to be approximately 0.13 m.



For comparison purposes, the pushover curves were re-computed using the refined FE model with two subdivisions through the thickness. The results for modes m1 and m3, the most important in terms of effective modal mass (Table 3), are reported in Figure 11, where the pushover curves (thick solid lines) are compared with those corresponding to the coarser discretization with one single subdivision through the thickness (thin solid lines). A very good agreement between the two FE models is shown in the plots.

### 3.4. Analysis of the 50 m high chimney

The original, 50 m high chimney (see [11]) is re-analyzed in detail in the present paper to compare its seismic response to that of the shortened chimney. All modes with effective mass larger than 4.5% of the total mass were used for the MPA. Therefore, lateral force profiles  $\mathbf{S}_n^*$ , with  $n$  alternatively taking the values 1, 2, 3, 5, and 6, were used, corresponding to the first five modes reported in Table 4. In analogy to the case of the shortened chimney, the amount of activated mass for the selected modes is approximately 71%.

The lateral load profiles, even in this case reproduced through body forces applied to the FEs, are reported in nondimensional form in Figure 8b. The corresponding pushover curves referred to the horizontal displacement of one of the nodes located at  $z = 50$  m are reported in Figure 9b, where open and solid circle data points have the same meaning as in Figure 9a. The target displacements  $u_{m0}$  for modes M1, M2 and M3 and ground motion scale factor  $SF_{ER} = 1$  are located beyond the elastic branch of the corresponding pushover curves, indicating that these modes may contribute to the damage pattern of the chimney. The total base shear obtained from the combination of the five modal contributions is 554 kN, approximately corresponding to 9.5% of the self weight. For  $SF_{ER} = 3$ , a significant contribution to the damage pattern is to be expected for all modes considered.

The peak modal displacements  $D_n$  for  $SF_{ER} = 1$  and 3 are reported in Figure 10b, where once again a close correlation with the values provided by the displacement response spectra is shown.

The lateral displacement profile obtained for the chimney from the MPA (SRSS combination rule) for  $SF_{ER} = 1$  is compared in Figure 9c (black dashed line) with that obtained for the shortened chimney. The maximum lateral displacement attained at the top resulted to be approximately 0.28 m.

### 3.5. Comparative analysis of the crack patterns

In the shortened chimney, the damage is mainly triggered by the fundamental mode. For the chimney model with one single subdivision through the thickness subjected to load profile  $s^*_1$  (mode m1), the damage evolution for increasing target displacements corresponding to scale factors  $SF_{ER} = 0.25, 0.38, 0.5, 0.75, 1, 1.5, 2$  and 3 is shown in Figure 12 in terms of tensile stress in the cracked elements. In particular, the damage is visualized by discs orthogonal to the local directions of crack opening. The cracks develop at elevations lying in the range 8–21 m. Because of its large masonry thickness, the base of the chimney turns out not to be damaged.

To observe a full development of higher-mode-induced damages, a high scale factor should be used. As an example, the damage maps obtained for load profiles  $s^*_2$  (mode m2),  $s^*_3$  (mode m3), and  $s^*_5$  (mode m5) with  $SF_{ER} = 3$  are reported in Figure 13a–c, whereas the combination (SRSS rule) of the tension damages produced by modes m1, m2, m3, and m5 for  $SF_{ER} = 3$  is represented in Figure 13d with a contour plot of the tensile stress.

For a better understanding of the damage evolution in the lower part of the stack, a detailed view of the damage pattern for mode m1 and  $SF_{ER} = 0.38$  (Figure 12b) is reported in Figure 14a. It can be noted by inspection that horizontal cracks develop on the upstream side of the chimney due to the presence of tensile stresses approximately parallel to the chimney stack. Conversely, on the downstream side of the chimney vertical cracks tend to develop along radial planes because of the tensile stresses in the tangential direction caused by the vertical compression.

The damage maps for the shortened chimney were recomputed for the refined model with two subdivisions through the thickness. For the fundamental mode, the damage patterns for  $SF_{ER} = 1$

and 3 are reported in Figures 14b and c, respectively, whereas Figure 14d refers to mode m3 and  $SF_{ER} = 3$ . A good agreement between the disc plots for the model with one single subdivision through the thickness (Figure 12e for m1 and  $SF_{ER} = 1$ , Figure 12h for m1 and  $SF_{ER} = 3$ , and Figure 13b for m3 and  $SF_{ER} = 3$ ) and the corresponding disc plots for the refined model (Figure 14b–d) is observed, confirming that the coarser discretization is sufficiently accurate for a damage analysis.

Differently from the shortened chimney, the higher-mode effects play a crucial role for the original chimney also for  $SF_{ER} = 1$ . The damage patterns for the 50 m high chimney obtained for lateral force distributions  $S^*_1$  (mode M1),  $S^*_2$  (mode M2), and  $S^*_3$  (mode M3) with  $SF_{ER} = 1$  are reported in the disc plots of Figure 15a–c (FE model with one single subdivision through the thickness), whereas the combination (SRSS rule) of these damages is represented with a contour plot in Figure 15d. The fundamental mode causes cracks in the bottom part of the stack, whereas modes M2 and M3 are the main responsible for the cracks produced at elevation lying in the ranges 28–42 m and 36–44 m, respectively. Note that the post-earthquake survey of the 50 m high chimney conducted in 2012 put in evidence diagonal cracks at an altitude of about 45 m (Figure 16). In the case of a ground motion scale factor  $SF_{ER} = 3$ , the higher-mode effects in the original chimney become even more evident (Figure 17), and damages in the upper part of the stack develop also for load profiles  $S^*_5$  (mode M5) and  $S^*_6$  (mode M6).

#### 4. Nonlinear response history analysis

The nonlinear RHA, i.e., the dynamic analysis of a given structure made of inelastic material and subjected to an acceleration time history, is the most advanced tool for the seismic risk assessment. For the general formulation of the method, see [44]. Differently from the MPA, that provides damage maps corresponding to the peak displacement attained during the earthquake (in the pushover analysis general method, the base shear-lateral displacement curve is assumed to represent the envelope of the loading cycles occurring during the seismic event), the RHA may be also used

for an evaluation of the damage at the end of the earthquake (permanent deformation, final crack configuration, etcetera).

In this section, the nonlinear RHA results obtained for the two chimneys are presented and discussed, in order to gain a deep insight into the seismic behavior of the structures under different ground motions. The accelerograms used in the analyses (Table 6) are real records corresponding to recent and less recent devastating seismic events occurred in Italy, New Zealand, and Japan, namely Irpinia (IR) and Emilia Romagna (ER), Christchurch (CH), and Niigata (NI). The axial symmetry of the chimneys allowed for the use of a single component of the horizontal ground motion.

For each seismic event considered, maximum horizontal component and vertical component, suitably scaled to obtain compatibility with the corresponding elastic response spectra provided in [26], were applied simultaneously in the analyses. The scale factors for the horizontal acceleration records are reported in the last column of Table 6, whereas the corresponding pseudo-acceleration spectra are compared in Figure 18 with the elastic spectrum provided by the Italian Building Code [26]. The choice of the various accelerograms was mainly motivated by their intensity in correspondence of the most significant vibration frequencies of the chimneys. For example, in correspondence of the fundamental period of the original chimney, ER ground motion yields an acceleration approximately 50% larger than the code spectrum (Figure 18a), whereas IR ground motion appears severe for the first (Figure 18a) and second (Figure 18b) modes of the shortened chimney. Analogously, CH and NI earthquakes are potentially expected to activate second and third modes of the original chimney (Figure 18b). The high values of horizontal acceleration associated with ER ground motion for periods lying in the range 1.5–2 s are a peculiar feature of the 2012 Emilia (Italy) seismic sequence, that resulted particularly severe for relatively flexible structures, such as precast RC buildings, bell towers and chimneys [45].

The lateral displacement time histories for a control node located on the top are reported in Figure 19a and in Figure 19b for the 37.6 m and the 50 m high chimney, respectively. The permanent lateral displacement at the end of the shaking is a typical damage indicator. For the

shortened chimney, the maximum permanent displacement, i.e.,  $u_{t,per,max} = 0.13$  m, was obtained for IR ground motion, and mean value and coefficient of variation (COV) of the permanent displacements obtained from the four analyses are  $u_{t,per,av} = 0.08$  m and  $COV_{u_{t,per}} = 45.5\%$ , respectively. The permanent displacement obtained for the original chimney is close to 0.10 m for IR and ER ground motions, and attains the maximum  $u_{t,per,max} = 0.17$  m for NI ground motion. In this case mean value and coefficient of variation are  $u_{t,per,av} = 0.12$  m and  $COV_{u_{t,per}} = 25.9\%$ , respectively. For all ground motions considered, the lateral displacement profiles corresponding to the maximum top displacements shown in Figure 19 are reported versus  $z$  in Figure 9c, where they are compared with the MPA results for  $SF_{ER} = 1$ . For both chimneys, the displacements obtained from the MPA are in excellent agreement with the RHA results for ER ground motion. For the shortened chimney, the maximum top displacement estimated from the MPA, i.e., 0.13 m, is close to the mean value obtained from the RHA for the four ground motions, equal to 0.11 m. Conversely, for the original chimney, the top displacements obtained from the MPA and the RHA for ER ground motion, i.e., 0.28 m and 0.30 m, are significantly larger than the mean value of the RHA results, equal to 0.21 m. These results confirm that ER ground motion was particularly severe for the 50 m high structure.

The damage maps in tension obtained from the RHA at five different time steps are reported in Figures 20 and 21 for the shortened chimney and in Figures 22 and 23 for the original chimney. The contour plots represented in these figures illustrate the damage in terms of parameter  $d_t$  appearing in Eq. (1), i.e., a scalar parameter varying from 0 (absence of damage) up to 1 (complete damage). The choice of plotting this parameter was essentially motivated by the interest in estimating the damage extent at the end of the four ground motions. Therefore, only a qualitative comparison in terms of damage localization can be made between the damage maps obtained from the RHA and those presented in Section 3.5, where the tensile stress in the damaged elements, vanishing when  $d_t$  tends to 1, is plotted.

With the exception of NI ground motion (Figure 20b), that mainly affects the intermediate-upper part of the structure, the shortened chimney presents damages widespread over the stack from  $z = 8$  m up to  $z = 32$  m. These damage maps indicate a contribution not only of the fundamental mode, but also of the higher modes of vibration, namely m2 and m3 in Figure 6. This behavior is only partly captured by the MPA, that for  $SF_{ER} = 1$  predicts damages in the lower part of the stack produced by the fundamental mode only, and suggests a possible damage spread up to  $z = 33$  m only for  $SF_{ER} = 3$  (Figure 13d).

The higher-mode effects play a crucial role for the 50 m high chimney, exhibiting damages mainly concentrated in the upper part of the stack. This is particularly evident for NI ground motion (Figure 22b). In all other simulations, depending on the particular accelerogram used, the damage tends to spread along the stack, but mostly affects the region between  $z = 30$  m and  $z = 44$  m. These results substantially confirm those presented in [11], where the 50 m high chimney was modelled using rigid triangular (2D) finite elements connected through nonlinear interfaces. An interesting correspondence is observed between the damage map obtained from the MPA for  $SF_{ER} = 1$  (Figure 15d) and that obtained from the RHA for ER ground motion (Figure 23a). In particular, the two methods of analysis locate the damages in the same parts of the stack, and highlight contributions of the fundamental and the higher modes clearly distinguishable from one another.

## 5. Conclusions

The results of a series of nonlinear analyses of a masonry chimney struck by the 2012 Emilia (Italy) seismic sequence are presented in the paper. At the time of the earthquakes, the chimney was 50 m high. After the second mainshock of the seismic sequence, the last 12 meters of the chimney were removed.

There is evidence that the current, 37.6 m high configuration of the chimney may correspond to that of the structure before the Second World War. In the Fifties, because of the expansion of the urban area of Ferrara, the chimney was probably raised up to a height of 50 m using a single course

of bricks of thickness 0.22 m. In this part of the structure, a noticeable material deterioration due to the atmospheric agents was observed in the aftermath of the 2012 Emilia earthquake's mainshocks. Therefore, the damages revealed after the seismic sequence probably resulted from the combined effect of poor conservation status and earthquake action. The real risk of partial collapses affecting the upper part of the stack, and the proximity to buildings hosting university classrooms and offices, led to the decision to disassemble the top 12 meters. The resulting structure, that is not substantially damaged, was analyzed in this work through a Modal Pushover Analysis (MPA) and nonlinear Response History Analyses (RHA) including both horizontal and vertical components of four real ground motions, suitably scaled to obtain compatibility with the elastic response spectra provided by the Italian Building Code. In the MPA, the target displacements locating the “modal” seismic demands were computed by means of the (horizontal component) inelastic response spectrum of the second mainshock of the Emilia earthquake sequence (ER ground motion), occurred on May 29, 2012 with  $M_w = 6.0$ .

In view of a possible reassembling of the removed part, the seismic behavior of the shortened chimney was compared with that of the original chimney. A preliminary analysis of this structure was presented in [11], where the computational model used for the RHA was based on two-dimensional finite elements. In the present work, the FE models adopted for the analyses were developed using 8-node solid elements. The constitutive model adopted for masonry takes account of different responses in tension and in compression, with suitable softening laws and a smoothed strength domain based on the Drucker-Prager criterion.

Two different commercial software packages were used for MPA and RHA. This aspect suggests that only a mainly qualitative comparison of the predictions provided by static and dynamic analyses can be made. Nevertheless, the masonry constitutive laws adopted for the RHA represent the extension to the cyclic load case of those used for the MPA. Well, a very good agreement between MPA and RHA was observed for the original chimney in terms of maximum lateral displacements and damage localization. This structure was shown to be particularly prone to

the higher-mode effects, with the stack region located at elevations between 30 and 44 m being susceptible to significant damages. The shortening had the effect of a strong reduction of the displacement demand: the MPA showed that the maximum lateral displacement decreases from 0.28 m for the original chimney up to about 0.13 m for the shortened structure. This feature, however, is not sufficient to deduce that shortening improved the seismic behavior. In fact, the total base shear, equal to 9.5% of the self weight for the 50 m high chimney, increases up to 14% of the self weight for the shortened chimney. The damage pattern of the shortened chimney highlighted by the RHA indicates that cracks may occur along a large part of the stack from  $z = 8$  m up to  $z = 33$  m, showing a not negligible contribution of the higher modes. In this case, the MPA only revealed damages in the lower part of the stack (8–21 m), because of the prevailing effects of the fundamental mode. This discrepancy must probably be ascribed to the contribution of the vertical component of the ground motion, that was taken into account in the RHA, but was ignored in the MPA. The maximum lateral displacement of the shortened chimney obtained from the MPA is close to the mean value of the maximum displacements obtained from the four dynamic analyses.

The dissipative capacity of the structures studied in the present paper is very low. For example, for the shortened chimney a weighted mean value of the strength reduction factor  $R$  approximately equal to 1.5 can be estimated from the MPA for  $SF_{ER} = 1$ , by using the effective modal masses as the weights. In fact, only the fundamental mode produces energy dissipation ( $R_1 > 1$ ), whereas for the higher modes the chimney remains within the elastic field ( $R_n = 1$  for  $n > 1$ ). Similar considerations can be made for the 50 m high chimney (see [11]), even if for this structure also  $R_2$ ,  $R_3 > 1$ . Therefore, were the masonry mechanical properties uniform in elevation, the 50 m high configuration would probably take advantage of a wider distribution of earthquake damages along the stack in comparison with the shortened chimney. The latter, indeed, is subjected to a damage concentration in the lower part of the stack. The possibility of reassembling the removed 12 meters should then be accurately considered, especially in the presence of specific recommendations of the Italian Ministry of Cultural Heritage.



In conclusion, the two analysis methods considered in the paper appear capable of predicting the main features of the seismic response of slender masonry chimneys, i.e., maximum displacement demand and damage localization. Only the RHA is able to predict permanent deformations and damage pattern at the end of the seismic event. For a preliminary damage assessment, the use of the MPA is suggested because of its lower computational effort.

## **Acknowledgements**

The present investigation was developed within the activities of the (Italian) University Network of Seismic Engineering Laboratories–ReLUIS in the research program funded by the Italian Civil Protection National Service – Progetto Esecutivo 2015 – Research Line “Masonry Structures”, WP2-WP4. A. Del Grosso and A. Tralli acknowledge the financial support of Foundation "Dr. Carlo Fornasini".

## **References**

- [1] Ghobarah A, Baumer T. Seismic response and retrofit of industrial brick masonry chimneys. *Canadian Journal of Civil Engineering* 1992; **19**(1): 117–128. DOI: 10.1139/192-012.
- [2] Riva P, Perotti F, Guidoboni E, Boschi E. Seismic analysis of the Asinelli Tower and earthquakes in Bologna. *Soil Dynamics and Earthquake Engineering* 1998; **17**(7–8): 525–550. DOI: [http://dx.doi.org/10.1016/S0267-7261\(98\)00009-8](http://dx.doi.org/10.1016/S0267-7261(98)00009-8).
- [3] Pallarés FJ, Aguero A, Martin M. Seismic behaviour of industrial masonry chimneys. *International Journal of Solids and Structures* 2006; **43**(7-8): 2076–2090. DOI: 10.1016/j.ijsolstr.2005.06.014.
- [4] Pallarés FJ, Aguero A, Ivorra S. A comparison of different failure criteria in a numerical seismic assessment of an industrial brickwork chimney. *Materials and Structures* 2009; **42**(2): 213–226. DOI: 10.1617/s11527-008-9379-5.

- [5] Pallarés FJ, Ivorra S, Pallarés L, Adam JM. Seismic assessment of a CFRP-strengthened masonry chimney. *Structures and Buildings* 2009; 162(5): 291–299. DOI: 10.1680/stbu.2009.162.5.291
- [6] Peña F, Lourenço PB, Mendes N, Oliveira DV. Numerical models for the seismic assessment of an old masonry tower. *Engineering Structures* 2010; 32(5): 1466–1478. DOI: 10.1016/j.engstruct.2010.01.027.
- [7] Pallarés FJ, Ivorra S, Pallarés L, Adam JM. State of the art of industrial masonry chimneys: A review from construction to strengthening. *Construction and Building Materials* 2011; 25(12): 4351–4361. DOI: doi:10.1016/j.conbuildmat.2011.02.004.
- [8] Ivorra S, Baeza FJ, Bru D, Varona FB. Seismic behavior of a masonry chimney with severe cracking condition: Preliminary study. *Key Engineering Materials* 2014; 628: 117–122. DOI: 10.4028/www.scientific.net/KEM.628.117.
- [9] Aoki T, Sabia D. Structural characterization of a brick chimney by experimental tests and numerical model updating. *Masonry International* 2006; 19: 41–52.
- [10] Aoki T, Sabia D, Rivella D. Influence of experimental data and FE model on updating results of a brick chimney. *Advances in Engineering Software* 2008; 39(4): 327–335. DOI: <http://dx.doi.org/10.1016/j.advengsoft.2007.01.005>.
- [11] Minghini F, Milani G, Tralli A. Seismic risk assessment of a 50 m high masonry chimney using advanced analysis techniques. *Engineering Structures* 2014; 69: 255–270. DOI: 10.1016/j.engstruct.2014.03.028.
- [12] European Committee for Standardization. *EN 1998-6:2005, Eurocode 8 – Design of structures for earthquake resistance – Part 6: Towers, masts and chimneys*. Brussels, Belgium, 2005.
- [13] Halabian AM, El Naggar MH. Effect of non-linear soil-structure interaction on seismic response of tall slender structures. *Soil Dynamics and Earthquake Engineering* 2002; 22(8): 639–658. DOI: [http://dx.doi.org/10.1016/S0267-7261\(02\)00061-1](http://dx.doi.org/10.1016/S0267-7261(02)00061-1).

- [14] Michel C, Gueguen P, Lestuzzi P. Observed non-linear soil-structure interaction from low amplitude earthquakes and forced-vibration recordings. In: *Proceedings of the 8th International Conference on Structural Dynamics* (Eurodyn 2011), Leuven, 2011, July 4–6.
- [15] Abu Zeid N, Rebecchi G, Tullini N, Laudiero F, Lanza L. Dynamic characterization of Medieval towers in the district of Ravenna (Italy). In: *Proceedings of the 12th Conference of the Italian National Association of Earthquake Engineering* (ANIDIS 2007), Pisa, 2007, June 10–14 (in Italian).
- [16] Cocchi C, Di Francesco C, Guidi F, Laudiero F, Minghini F, Rebecchi G, Tullini N. Seismic vulnerability assessment for the Basilica and bell tower of Sant'Apollinare in Classe (Ravenna), Italy. *Ingenio* 2014; **26**. Dossier on Restoration and Strengthening, available at [http://www.ingenio-web.it/Rivista/107/INGENIO\\_n.26.html](http://www.ingenio-web.it/Rivista/107/INGENIO_n.26.html) (in Italian).
- [17] Pais A, Kausel E. Approximate formulas for dynamic stiffnesses of rigid foundation. *Soil Dynamics and Earthquake Engineering* 1988; 7(4): 213–227. DOI: 10.1016/S0267-7261(88)80005-8.
- [18] Sabia D, Aoki T, Cosentini RM, Lancellotta R. Model updating to forecast the dynamic behavior of the Ghirlandina Tower in Modena, Italy. *Journal of Earthquake Engineering* 2015; **19**(1): 1–24. DOI: 10.1080/13632469.2014.962668.
- [19] DIANA Finite Element Analysis, Release 9.5. *User's Manual*. TNO DIANA BV: Delft, 2013.
- [20] ABAQUS Finite Element Analysis, Release 6.6. *Theory Manual*. SIMULIA, Inc.: Maastricht, 2006.
- [21] Rots JG, Blaauwendraad J. Crack models for concrete: Discrete or smeared? Fixed, multi-directional or rotating? *HERON Journal* 1989; **34**(1): 1–59.
- [22] Lourenço PB. *Computational strategies for masonry structures*. Ph.D. Dissertation, Delft University of Technology: Delft, 1996.

- [23] Casolo S, Milani G, Uva G, Alessandri, C. Comparative seismic vulnerability analysis on ten masonry towers in the coastal Po Valley in Italy. *Engineering Structures* 2013; **49**: 465–490. DOI: 10.1016/j.engstruct.2012.11.033.
- [24] Scotta R, Vitaliani R, Saetta A, Oñate E, Hanganu A. A scalar damage model with a shear retention factor for the analysis of reinforced concrete structures: theory and validation. *Computer and Structures* 2001; **79**(7): 737–755.
- [25] European Committee for Standardization. *EN 1998-3:2005, Eurocode 8 – Design of structures for earthquake resistance – Part 3: Assessment and retrofitting of buildings*. Brussels, Belgium, 2005.
- [26] Italian Ministry of Infrastructure and Transport. *Italian Building Code-D.M. 14/01/2008*. Rome, Italy, 2008 (in Italian).
- [27] Lee J, Fenves GL. Plastic-damage model for cyclic loading of concrete structures. *Journal of Engineering Mechanics* 1998; **124**(8): 892–900.
- [28] Majewski S. *The mechanics of structural concrete in terms of elasto-plasticity*. Silesian Polytechnic Publishing House: Gliwice, 2003.
- [29] William KJ, Warnke EP. Constitutive models for the triaxial behavior of concrete. In: *Proceedings of the International Association for Bridge and Structural Engineering* 1975, Vol 19: 1–30.
- [30] Van Zijl G. Modeling Masonry Shear-Compression: Role of Dilatancy Highlighted. *Journal of Engineering Mechanics ASCE* 2004; **130**(11): 1289–1296. DOI: [http://dx.doi.org/10.1061/\(ASCE\)0733-9399\(2004\)130:11\(1289\)](http://dx.doi.org/10.1061/(ASCE)0733-9399(2004)130:11(1289)).
- [31] Page A. The biaxial compressive strength of brick masonry. *Proceedings of the Institution of Civil Engineers* 1981; **71**: 893–906.
- [32] Lubliner J, Oliver J, Oller S, Oñate E. A plastic-damage model for concrete, *International Journal of Solids Structures* 1989; **25**(3): 299-326. DOI: 10.1016/0020-7683(89)90050-4.

- [33] Chopra AK, Goel RK. A modal pushover analysis procedure for estimating seismic demands for buildings. *Earthquake Engineering and Structural Dynamics* 2002; **31**(3): 561–582. DOI: 10.1002/eqe.144.
- [34] Chopra AK. *Dynamics of Structures. Theory and Applications to Earthquake Engineering*. Prentice Hall: Upper Saddle River, 2001 (2nd ed.).
- [35] Goel RK, Chopra AK. Evaluation of Modal and FEMA Pushover Analyses: SAC Buildings. *Earthquake Spectra* 2004; **20**(1): 225–254. DOI: 10.1193/1.1646390.
- [36] Goel RK, Chopra AK. Extension of Modal Pushover Analysis to Compute Member Forces. *Earthquake Spectra* 2005; **21**(1): 125–139. DOI: 10.1193/1.1851545.
- [37] Chopra AK, Goel RK, Chintanapakdee C. Evaluation of a modified MPA procedure assuming higher modes as elastic to estimate seismic demands. *Earthquake Spectra* 2004; **20**(3): 757–778. DOI: 10.1193/1.1775237.
- [38] Chopra AK, Goel RK. Role of Higher-"Mode" Pushover Analyses in Seismic Analysis of Buildings. *Earthquake Spectra* 2005; **21**(4): 1027–1041. DOI: 10.1193/1.2085189.
- [39] Reyes JC, Chopra AK. Three-dimensional modal pushover analysis of buildings subjected to two components of ground motion, including its evaluation for tall buildings. *Earthquake Engineering and Structural Dynamics* 2011; **40**(7): 789–806. DOI: 10.1002/eqe.1060.
- [40] Reyes JC, Chopra AK. Evaluation of three-dimensional modal pushover analysis for unsymmetric-plan buildings subjected to two components of ground motion. *Earthquake Engineering and Structural Dynamics* 2011; **40**(13): 1475–1494. DOI: 10.1002/eqe.1100.
- [41] Kalkan E, Chopra AK. Modal-pushover-based ground-motion scaling procedure. *Journal of Structural Engineering* 2011; **137**(3): 298–310. DOI: 10.1061/(ASCE)ST.1943-541X.0000308.

- [42] Reyes JC, Chopra AK. Modal pushover-based scaling of two components of ground motion records for nonlinear RHA of buildings. *Earthquake Spectra* 2012; **28**(3): 1243–1267. DOI: 10.1193/1.4000069.
- [43] Reyes JC, Quintero OA. Modal pushover-based scaling of earthquake records for nonlinear analysis of single-story unsymmetric-plan buildings. *Earthquake Engineering and Structural Dynamics* 2014; **43**(7): 1005–1021. DOI: 10.1002/eqe.2384.
- [44] Wilson EL, Farhoomand I, Bathe KJ. Nonlinear dynamic analysis of complex structures. *Earthquake Engineering & Structural Dynamics* 1972; **1**(3): 241–252.
- [45] Mucciarelli M, Liberatore D. Guest editorial: The Emilia 2012 earthquakes, Italy. *Bulletin of Earthquake Engineering* 2014; **12**(5): 2111–2116. DOI: 10.1007/s10518-014-9629-6.

## Table Captions

Table 1. Chimney's geometry.

Table 2. Material properties used in the pushover analyses.

Table 3. Shortened chimney, results of the frequency analysis for the first six flexural mode shapes obtained for the FE model with one single subdivision through the thickness.

Table 4. Original chimney, results of the frequency analysis for the first six flexural mode shapes (FE model with one single subdivision through the thickness).

Table 5. Shortened chimney, frequencies and effective modal masses for the first six flexural mode shapes obtained for the FE model with two subdivisions through the thickness, and comparisons with second and fourth columns of Table 3.

Table 6. Ground motions used in the RHA and corresponding moment magnitudes ( $M_w$ ); fault mechanisms; ground types; epicentral distances of the recording station ( $R_{epi}$ ); and scale factors ( $SF$ ) to be applied to the maximum horizontal component to obtain compatibility with elastic spectrum provided by [26].

## Figure Captions

Figure 1. The chimney (a) after and (b) before shortening.

Figure 2. Shear behavior adopted in the pushover analyses for uncracked (dashed line) and cracked (solid line) masonry.

Figure 3. Representation of the masonry constitutive behavior in (a) tension and (b) compression.

Figure 4. ABAQUS modified Drucker-Prager strength domain.

Figure 5. Smoothed Drucker-Prager failure criterion adopted in the simulations,  $q$ - $p$  plane.

Figure 6. Mode shapes of the shortened chimney (corresponding natural frequencies reported in Table 3).

Figure 7. Mode shapes of the chimney before shortening (corresponding natural frequencies reported in Table 4).

Figure 8. Lateral load patterns (a)  $\mathbf{s}_n^*$  and (b)  $\mathbf{S}_n^*$  used for the MPA of shortened and original chimney, respectively.

Figure 9. Pushover curves for (a) the shortened, and (b) the original chimney; and (c) final profiles of the lateral displacement obtained from the analyses. Open and solid circle data points in Figure 9a,b locate the target displacements obtained from Eq. (3) by assuming a ground motion scale factor  $SF_{ER} = 1$  and 3, respectively.



Figure 10. Displacement spectra for the East-West component of ER ground motion scaled with factors  $SF_{ER} = 1$  and 3. Open and solid circle data points refer to maximum displacements  $D_n$  of the SDOF inelastic systems for (a) the shortened, and (b) the original chimney.

Figure 11. Pushover curves for the shortened chimney corresponding to load profiles (a)  $\mathbf{s}_1^*$  (mode m1); and (b)  $\mathbf{s}_3^*$  (mode m3). Comparison between FE models with one single and two subdivisions through the thickness.

Figure 12. Shortened chimney, downstream (close-up view) and upstream sides: disc plots representing the crack patterns in terms of tensile stress (in  $N/m^2$ ) obtained from the pushover analysis with load profile  $\mathbf{s}_1^*$  (mode m1). Damage evolution related to ER ground motion scale factors (a)  $SF_{ER} = 0.25$ , (b) 0.38, (c) 0.5, (d) 0.75, (e) 1, (f) 1.5, (g) 2, and (h) 3.

Figure 13. (a-c) Shortened chimney, downstream (close-up view) and upstream sides: disc plots representing the crack patterns in terms of tensile stress (in  $N/m^2$ ) obtained from the pushover analysis with load profiles (a)  $\mathbf{s}_2^*$  (mode m2), (b)  $\mathbf{s}_3^*$  (mode m3), and (c)  $\mathbf{s}_5^*$  (mode m5) for ER ground motion scale factor  $SF_{ER} = 3$ ; (d) contour plot of the tensile stress in the cracked elements representing the combination of tension damages produced by modes m1 (Figure 12h), m2, m3 and m5 for  $SF_{ER} = 3$ .

Figure 14. Shortened chimney. (a) Detail of Figure 12b, and disc plots of the tensile stress in the cracked elements (in  $N/m^2$ ) obtained from the MPA for the model with two subdivisions through the thickness (upstream side of the chimney) in the cases: (b) mode m1 and  $SF_{ER} = 1$ ; (c) mode m1 and  $SF_{ER} = 3$ ; and, finally, (d) mode m3 and  $SF_{ER} = 3$ .

Figure 15. (a-c) Original chimney, downstream (close-up view) and upstream sides: disc plots representing the crack patterns in terms of tensile stress (in  $\text{N/m}^2$ ) obtained from the pushover analysis with load profiles (a)  $\mathbf{S}^*_1$  (mode M1), (b)  $\mathbf{S}^*_2$  (mode M2), and (c)  $\mathbf{S}^*_3$  (mode M3) for ER ground motion scale factor  $SF_{ER} = 1$ ; (d) contour plot of the tensile stress in the cracked elements representing the combination of tension damages produced by modes M1, M2 and M3 for  $SF_{ER} = 1$ .

Figure 16. Diagonal cracks observed after Emilia earthquake's main shocks.

Figure 17. (a-e) Original chimney, downstream (close-up view) and upstream sides: disc plots representing the crack patterns in terms of tensile stress (in  $\text{N/m}^2$ ) obtained from the pushover analysis with load profiles (a)  $\mathbf{S}^*_1$  (mode M1), (b)  $\mathbf{S}^*_2$  (mode M2), (c)  $\mathbf{S}^*_3$  (mode M3), (d)  $\mathbf{S}^*_5$  (mode M5), and (e)  $\mathbf{S}^*_6$  (mode M6) for ER ground motion scale factor  $SF_{ER} = 3$ ; (f) contour plot of the tensile stress in the cracked elements representing the combination of tension damages produced by modes M1, M2, M3, M5 and M6 for  $SF_{ER} = 3$ .

Figure 18. (a) Pseudo-acceleration response spectra of the maximum horizontal component for ground motions reported in Table 6 and elastic spectrum provided by [25]. The ground motions are scaled by the factors reported in the last column of Table 6. (b) Detail of the spectra for the period lying in the range 0–1 s.  $T_{i,38}$  ( $i = 1, \dots, 3$ ) and  $T_{j,50}$  ( $j = 1, \dots, 3, 5$ ) indicate the first three natural periods of the shortened chimney (Table 3) and the first four natural periods of the original chimney (Table 4).

Figure 19. Top displacement time histories for (a) the shortened and (b) the original chimney.

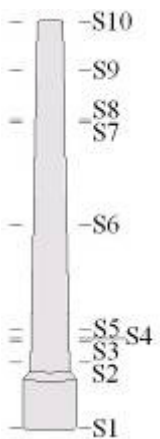
Figure 20. Shortened chimney: damage maps in tension at different time steps for (a) CH and (b) NI ground motions.

Figure 21. Shortened chimney: damage maps in tension at different time steps for (a) ER and (b) IR ground motions.

Figure 22. Original chimney: damage maps in tension at different time steps for (a) CH and (b) NI ground motions.

Figure 23. Original chimney: damage maps in tension at different time steps for (a) ER and (b) IR ground motions.

Table 1. Chimney's geometry.



	Cross-section	Position along the vertical axis, $z$ (m)	Outer diameter $\varnothing_{out}$ (m)	Wall thickness $t$ (m)
	S1	0.0	6.61	1.80
	S2	8.0	4.30	0.95
	S3	10.5	4.24	0.95
	S4	11.0	4.22	0.50
	S5	12.0	4.19	0.28
	S6	25.0	3.77	0.28
	S7	37.6	3.38	0.28
	S8	38.0	3.37	0.22
	S9	44.0	3.21	0.22
	S10	50.0	3.19	0.22

Table 2. Material properties used in the pushover analyses.

Young's modulus	Poisson's ratio	Strengths Compressive	Tensile	Ultimate tensile strain	Shear retention factor
$E$	$\nu$	$f_c$	$f_t$	$\epsilon_t$	$\beta$
MPa		MPa	MPa	‰	
1500	0.15	3.5	0.1	0.5	0.05

Table 3. Shortened chimney, results of the frequency analysis for the first six flexural mode shapes obtained for the FE model with one single subdivision through the thickness.

Mode	Frequency $f_n$ (Hz)	Period $T_n$ (s)	Effective modal mass/Total mass $M_n^*/M$ (%)	Participation factor $\Gamma_n$
m1	0.85	1.18	19.52	1.68
m2	3.92	0.26	14.58	1.36
m3	8.07	0.12	23.81	1.45
m5	12.06	0.08	12.88	1.14
m6	18.06	0.06	4.93	0.68
m8	24.17	0.04	5.47	0.62
Total activated mass			81.19	

Table 4. Original chimney, results of the frequency analysis for the first six flexural mode shapes (FE model with one single subdivision through the thickness).

Mode	Frequency $f_n$ (Hz)	Period $T_n$ (s)	Effective modal mass/Total mass $M_n^*/M$ (%)	Participation factor $\Gamma_n$
M1	0.46	2.16	20.58	1.73
M2	2.16	0.46	10.62	1.31
M3	5.03	0.20	10.56	1.23
M5	8.13	0.12	17.60	1.35
M6	11.19	0.09	11.51	1.14
M7	15.26	0.07	4.33	0.74
Total activated mass			75.20	

Table 5. Shortened chimney, frequencies and effective modal masses for the first six flexural mode shapes obtained for the FE model with two subdivisions through the thickness, and comparisons with second and fourth columns of Table 3.

Mode	Frequency $f_{n,2}$ (Hz)	Effective modal mass/Total mass $M_{n,2}^*/M$ (%)	Percentage differences	
			$100 \times  f_{n,2} - f_n  / f_{n,2}$ (%)	$100 \times  M_{n,2}^* - M_n^*  / M_{n,2}^*$ (%)
m1	0.84	19.52	0.086	0.041
m2	3.92	14.52	0.016	0.365
m3	8.08	23.81	0.218	0.013
m5	12.08	13.20	0.152	2.461
m6	18.07	5.05	0.083	2.436
m8	24.20	5.43	0.137	0.718

Table 6. Ground motions used in the RHA and corresponding moment magnitudes ( $M_w$ ); fault mechanisms; ground types; epicentral distances of the recording station ( $R_{epi}$ ); and scale factors ( $SF$ ) to be applied to the maximum horizontal component to obtain compatibility with elastic spectrum provided by [25].

Event No.	Event site	Label	Date	$M_w$	Fault mech.	Ground type	$R_{epi}$ (km)	$SF$
1	Christchurch (New Zealand)	CH	2011-02-21	6.2	Reverse	C	14	0.7
2	Irpinia (Italy)	IR	1980-11-23	6.9	Normal	A	24	3.6
3	Niigata (Japan)	NI	2004-10-23	6.3	Reverse	C	17	0.6
4	Emilia (Italy)	ER	2012-05-29	6.0	Reverse	C	5	$\approx 1$



a



b

Figure 1. The chimney (a) after and (b) before shortening.

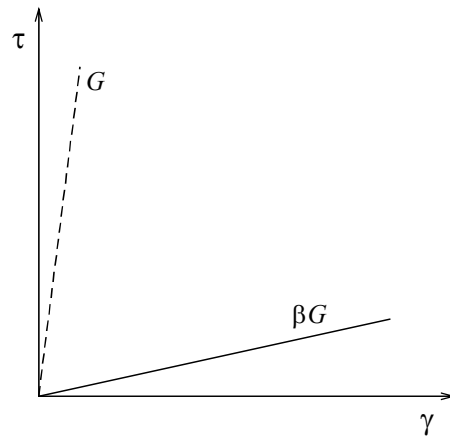


Figure 2. Shear behavior adopted in the pushover analyses for uncracked (dashed line) and cracked (solid line) masonry.

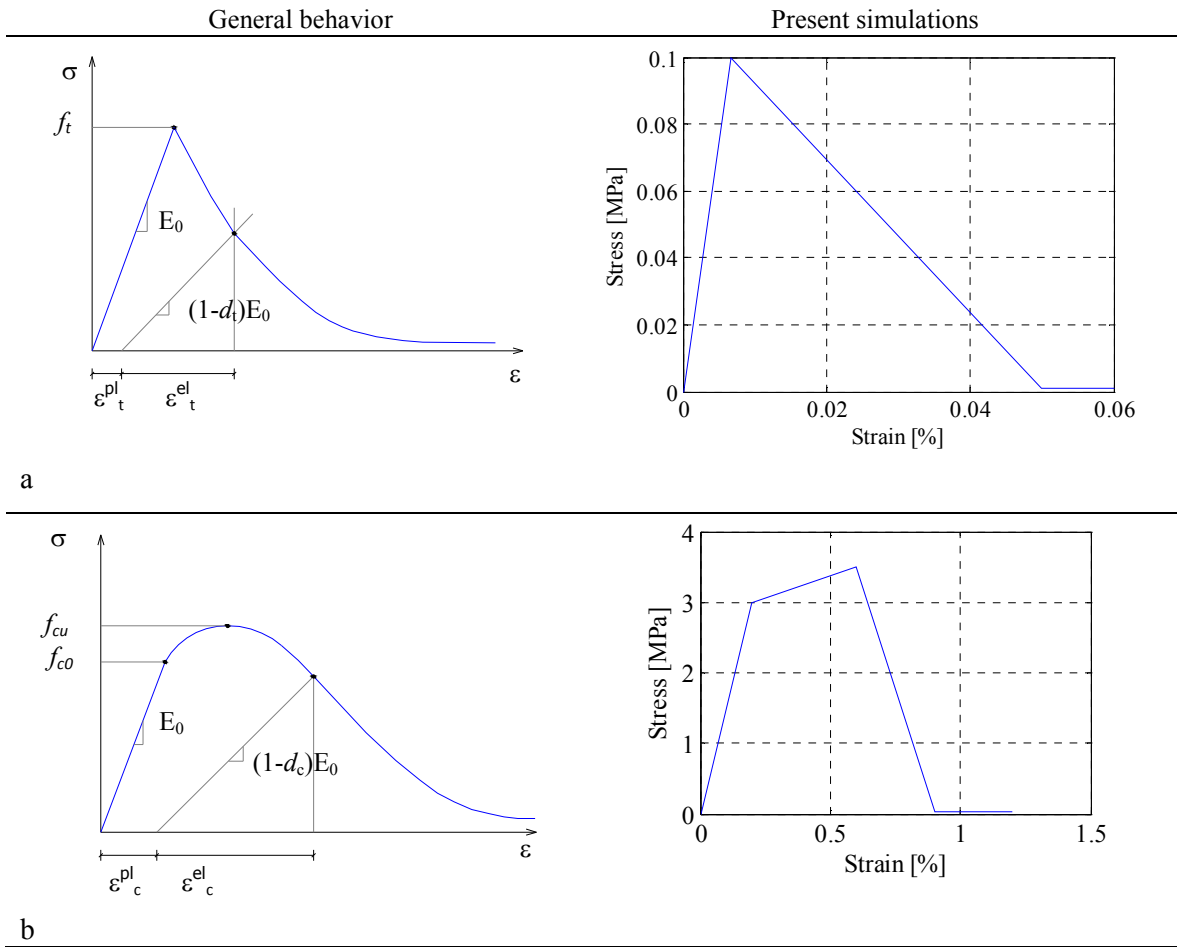


Figure 3. Representation of the masonry constitutive behavior in (a) tension and (b) compression.



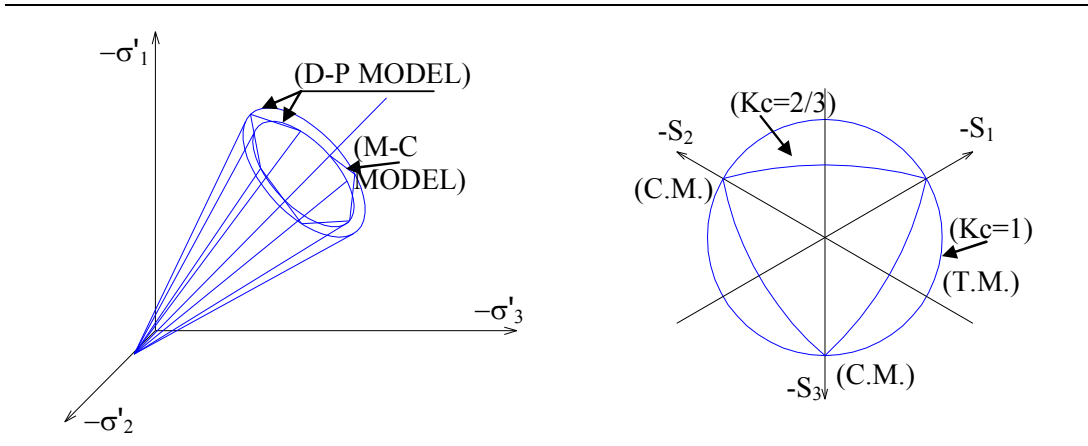


Figure 4. ABAQUS modified Drucker-Prager strength domain.

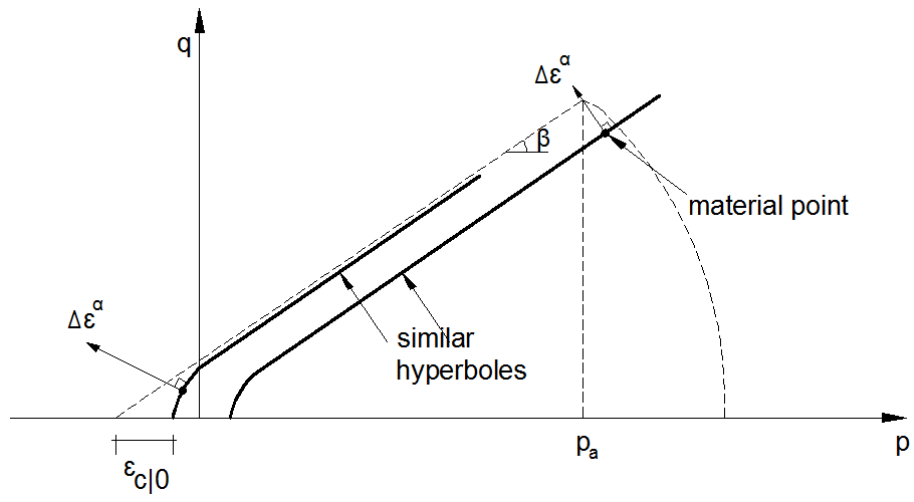


Figure 5. Smoothed Drucker-Prager failure criterion adopted in the simulations,  $q$ - $p$  plane.

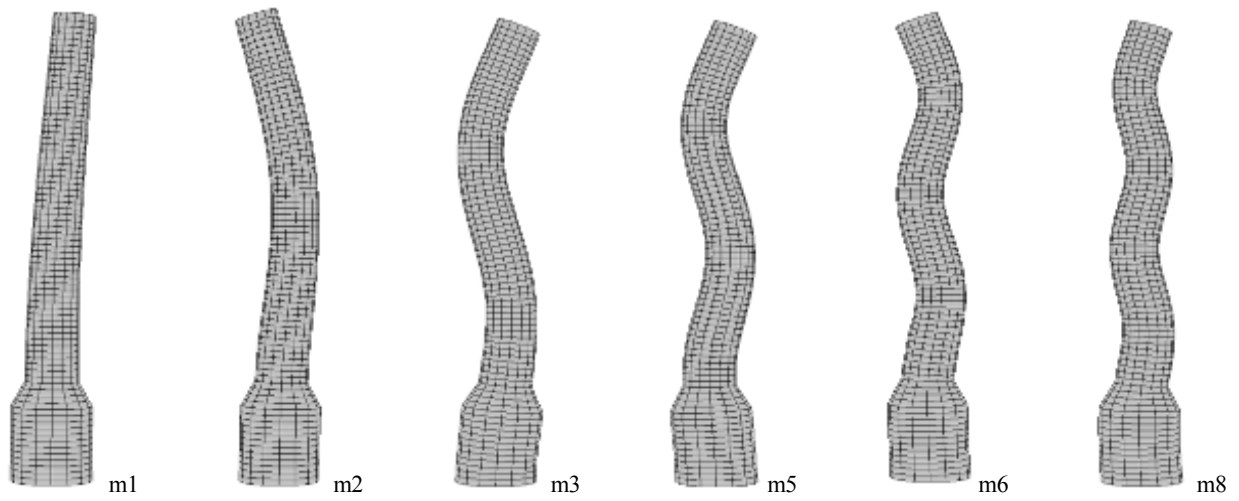


Figure 6. Mode shapes of the shortened chimney (corresponding natural frequencies reported in Table 3).

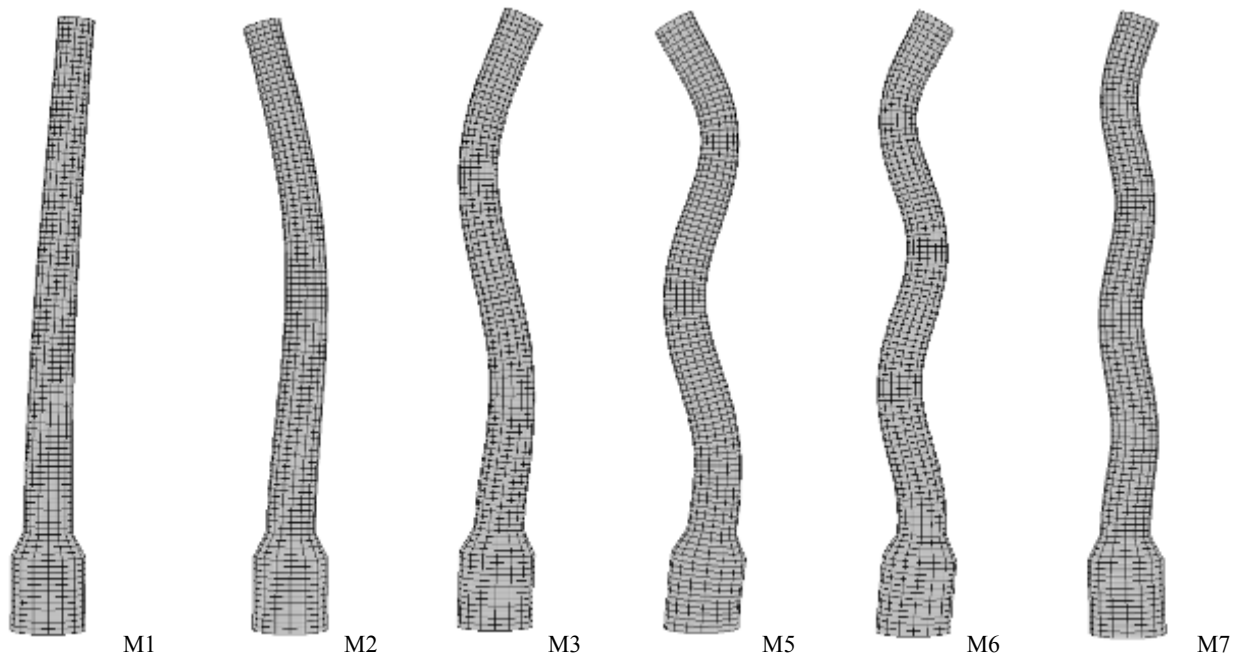


Figure 7. Mode shapes of the chimney before shortening (corresponding natural frequencies reported in Table 4).

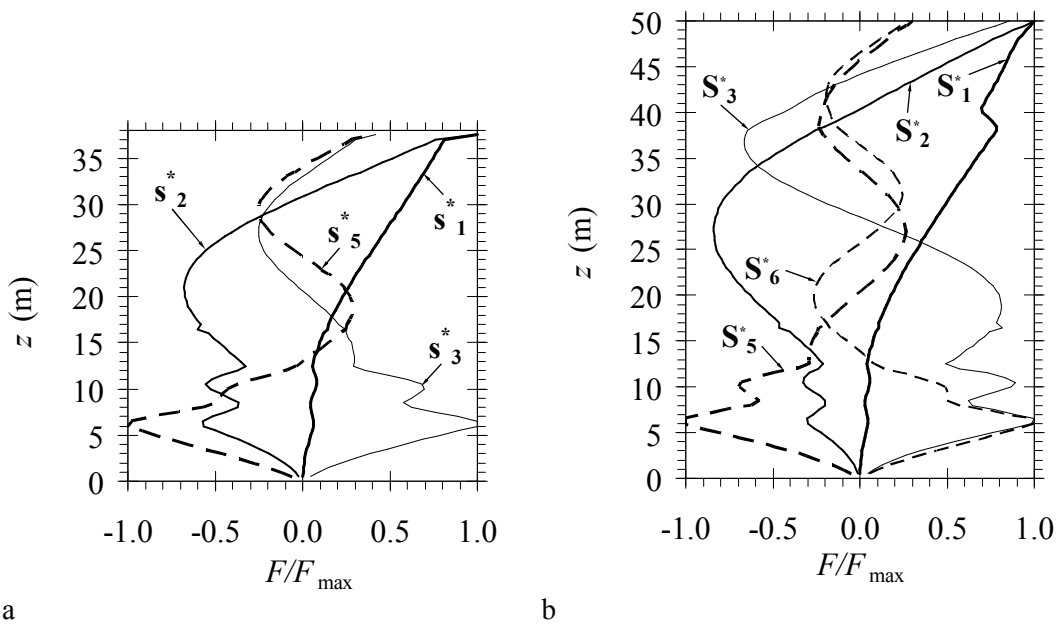


Figure 8. Lateral load patterns (a)  $s_n^*$  and (b)  $S_n^*$  used for the MPA of shortened and original chimney, respectively.

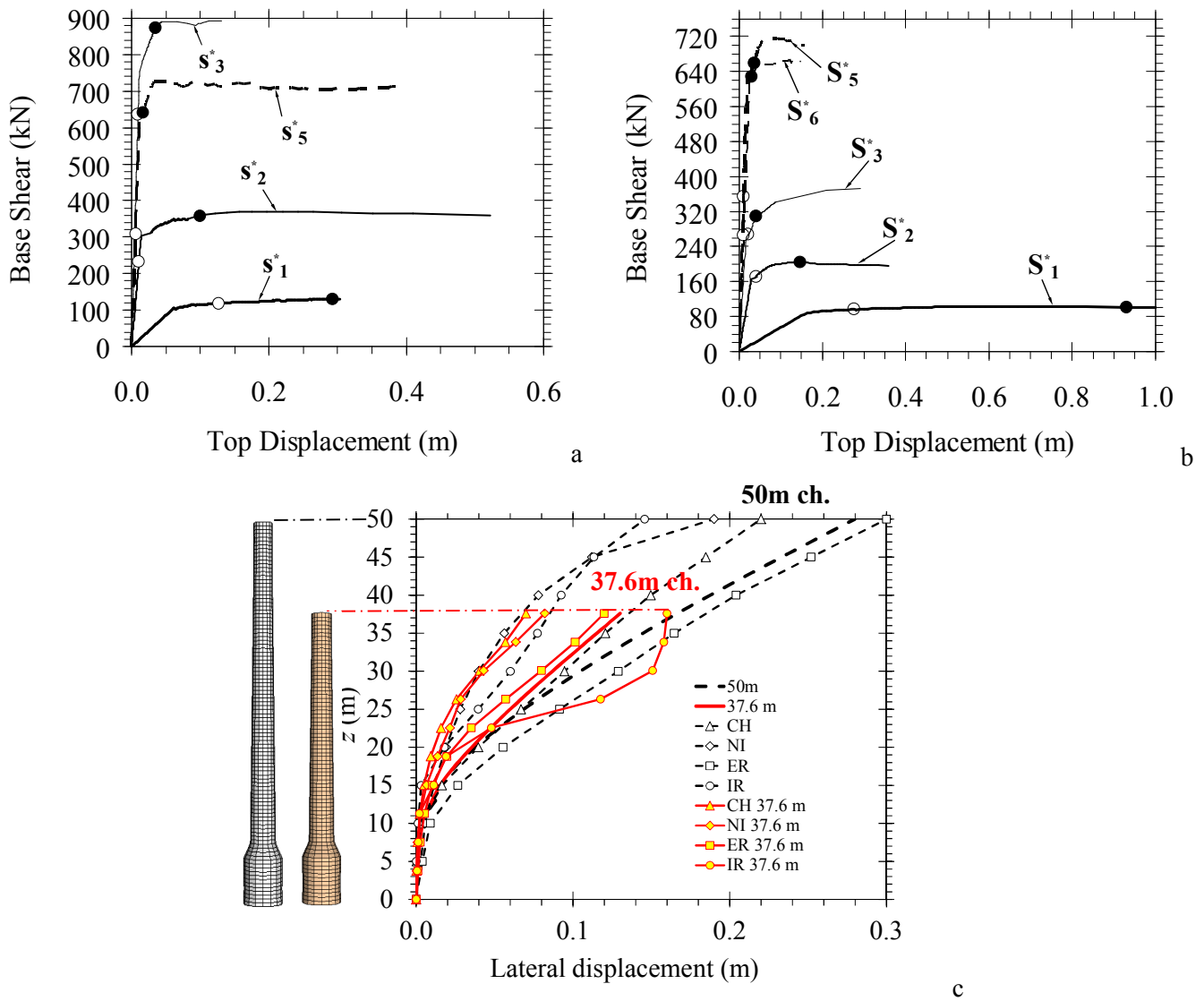


Figure 9. Pushover curves for (a) the shortened, and (b) the original chimney; and (c) final profiles of the lateral displacement obtained from the analyses. Open and solid circle data points in Fig. 9a,b locate the target displacements obtained from Eq. (3) by assuming a ground motion scale factor  $SF_{ER} = 1$  and 3, respectively.

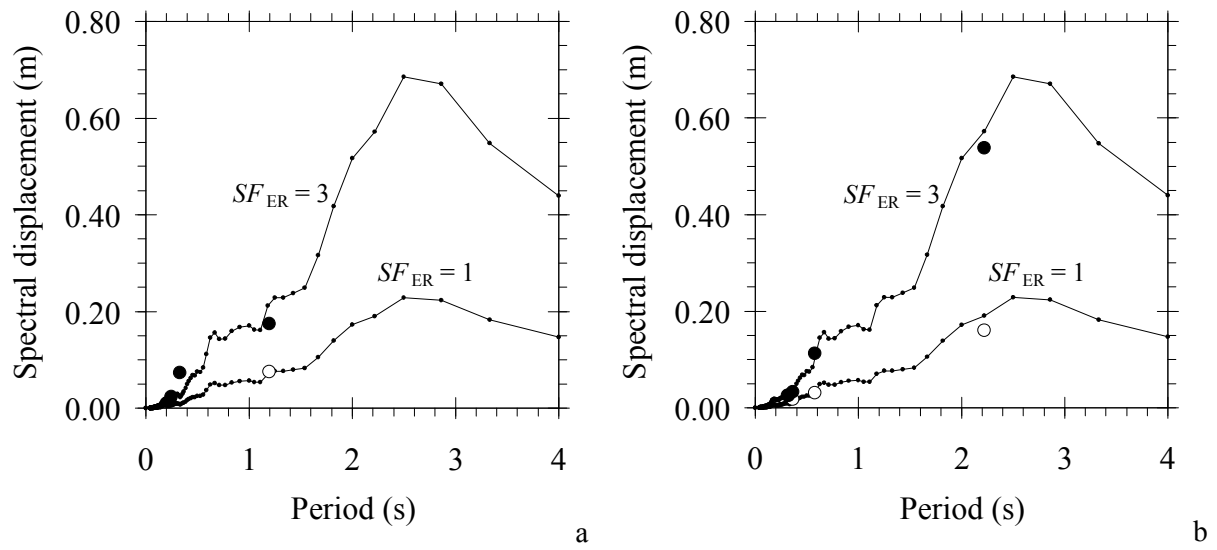
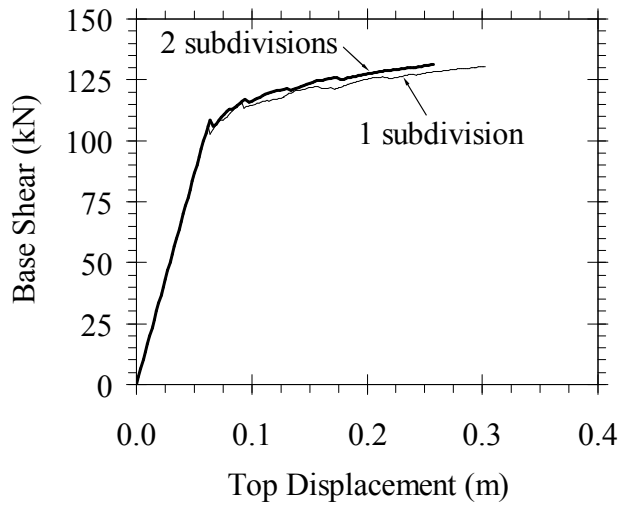
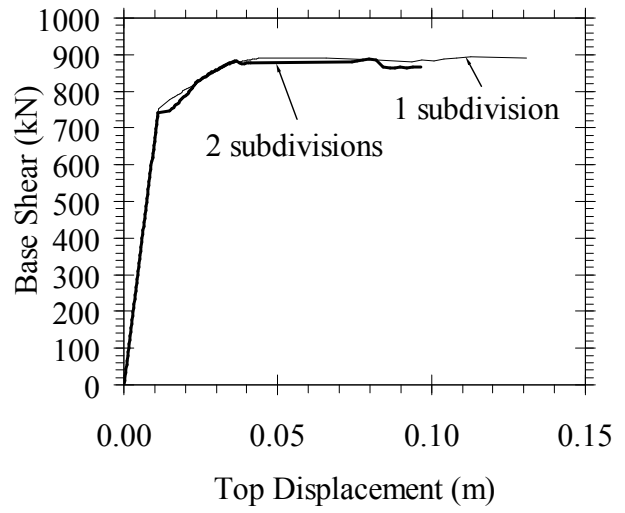


Figure 10. Displacement spectra for the East-West component of ER ground motion scaled with factors  $SF_{ER} = 1$  and 3. Open and solid circle data points refer to maximum displacements  $D_n$  of the SDOF inelastic systems for (a) the shortened and (b) the original chimneys.



a



b

Figure 11. Pushover curves for the shortened chimney corresponding to load profiles (a)  $\mathbf{s}_1^*$  (mode m1); and (b)  $\mathbf{s}_3^*$  (mode m3). Comparison between FE models with one single and two subdivisions through the thickness.



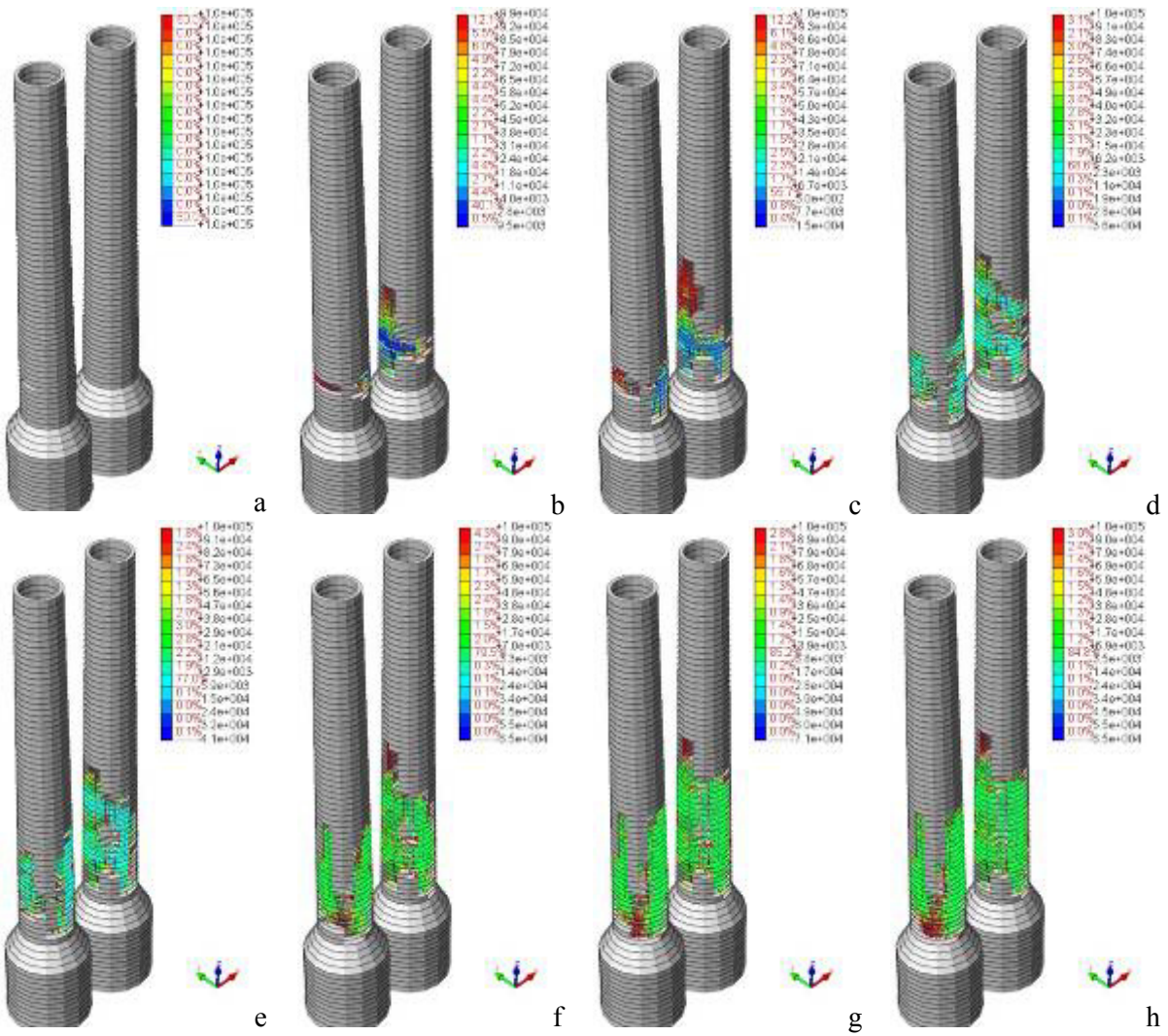


Figure 12. Shortened chimney, downstream (close-up view) and upstream sides: disc plots representing the crack patterns in terms of tensile stress (in  $N/m^2$ ) obtained from the pushover analysis with load profile  $\dot{s}_1$  (mode m1). Damage evolution related to ER ground motion scale factors (a)  $SF_{ER} = 0.25$ , (b) 0.38, (c) 0.5, (d) 0.75, (e) 1, (f) 1.5, (g) 2, and (h) 3.

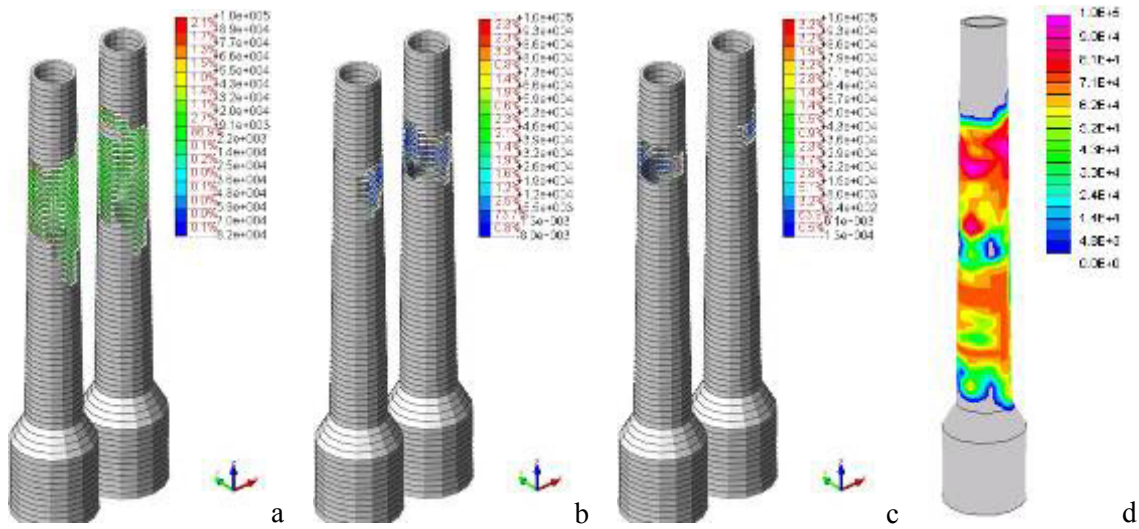


Figure 13. (a-c) Shortened chimney, downstream (close-up view) and upstream sides: disc plots representing the crack patterns in terms of tensile stress (in  $N/m^2$ ) obtained from the pushover analysis with load profiles (a)  $s^*_2$  (mode m2), (b)  $s^*_3$  (mode m3), and (c)  $s^*_5$  (mode m5) for ER ground motion scale factor  $SF_{ER} = 3$ ; (d) contour plot of the tensile stress in the cracked elements representing the combination of tension damages produced by modes m1 (Fig. 12h), m2, m3 and m5 for  $SF_{ER} = 3$ .

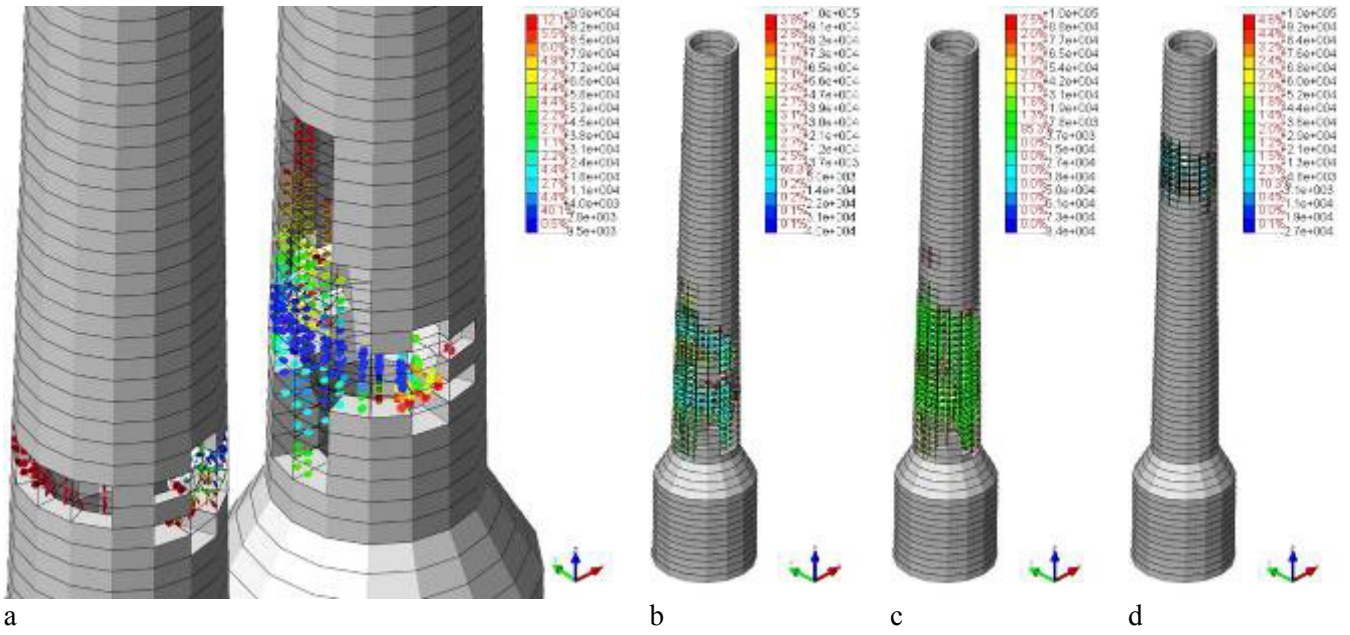


Figure 14. Shortened chimney. (a) Detail of Fig. 12b, and disc plots of the tensile stress in the cracked elements (in  $N/m^2$ ) obtained from the MPA for the model with two subdivisions through the thickness (upstream side of the chimney) in the cases: (b) mode m1 and  $SF_{ER} = 1$ ; (c) mode m1 and  $SF_{ER} = 3$ ; and, finally, (d) mode m3 and  $SF_{ER} = 3$ .

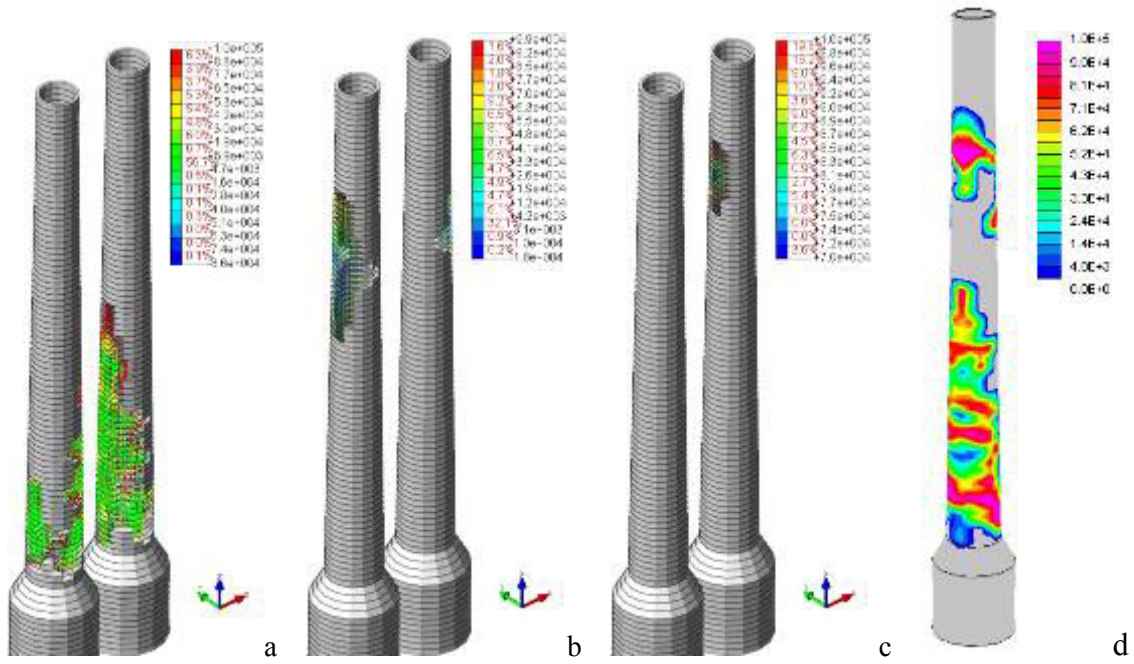


Figure 15. (a-c) Original chimney, downstream (close-up view) and upstream sides: disc plots representing the crack patterns in terms of tensile stress (in  $\text{N/m}^2$ ) obtained from the pushover analysis with load profiles (a)  $S_1^*$  (mode M1), (b)  $S_2^*$  (mode M2), and (c)  $S_3^*$  (mode M3) for ER ground motion scale factor  $SF_{ER} = 1$ ; (d) contour plot of the tensile stress in the cracked elements representing the combination of tension damages produced by modes M1, M2 and M3 for  $SF_{ER} = 1$ .

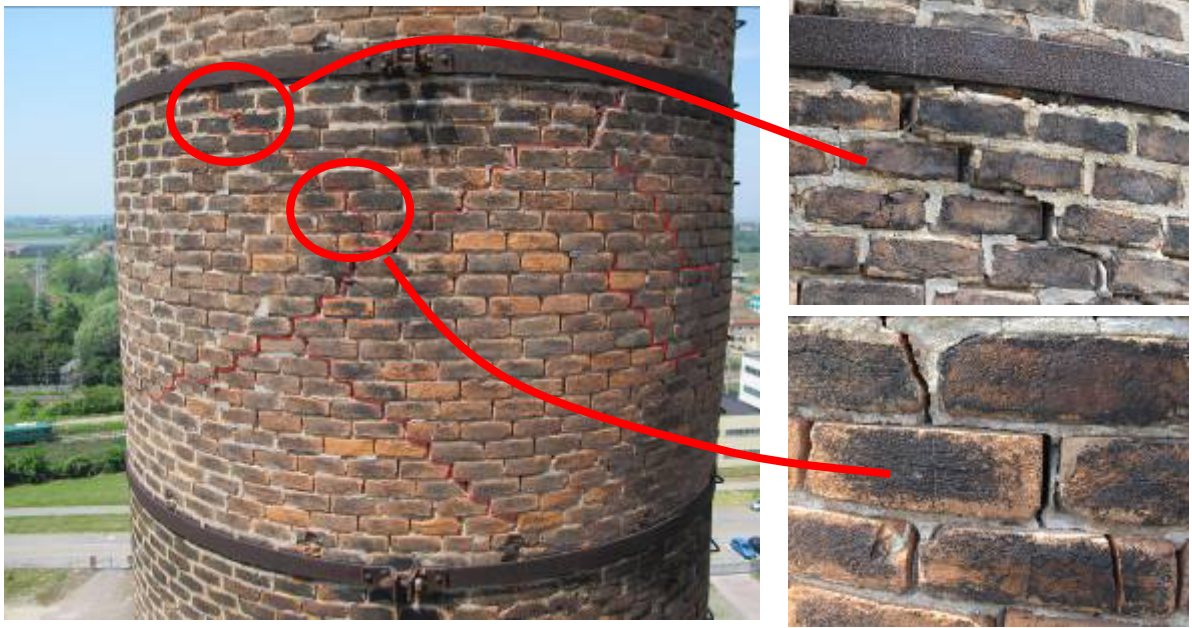


Figure 16. Diagonal cracks observed after Emilia earthquake's main shocks.



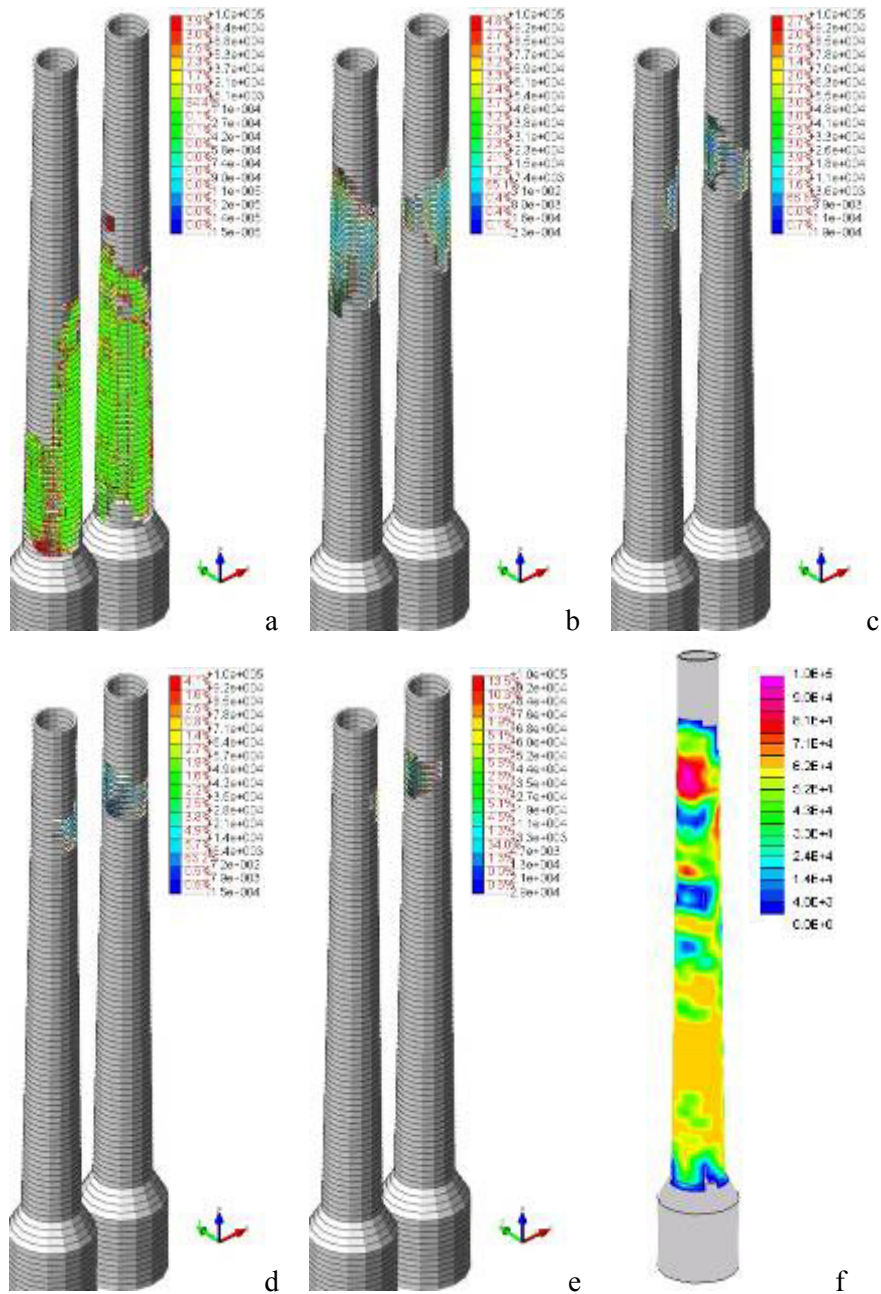


Figure 17. (a-e) Original chimney, downstream (close-up view) and upstream sides: disc plots representing the crack patterns in terms of tensile stress (in  $N/m^2$ ) obtained from the pushover analysis with load profiles (a)  $S_1^*$  (mode M1), (b)  $S_2^*$  (mode M2), (c)  $S_3^*$  (mode M3), (d)  $S_5^*$  (mode M5), and (e)  $S_6^*$  (mode M6) for ER ground motion scale factor  $SF_{ER} = 3$ ; (f) contour plot of the tensile stress in the cracked elements representing the combination of tension damages produced by modes M1, M2, M3, M5 and M6 for  $SF_{ER} = 3$ .

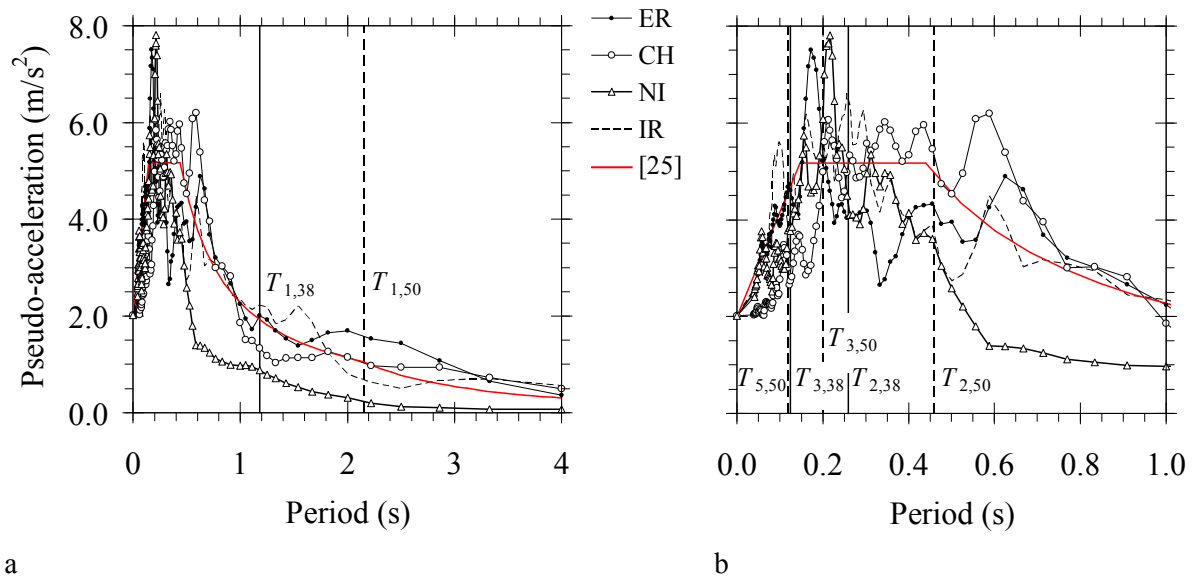
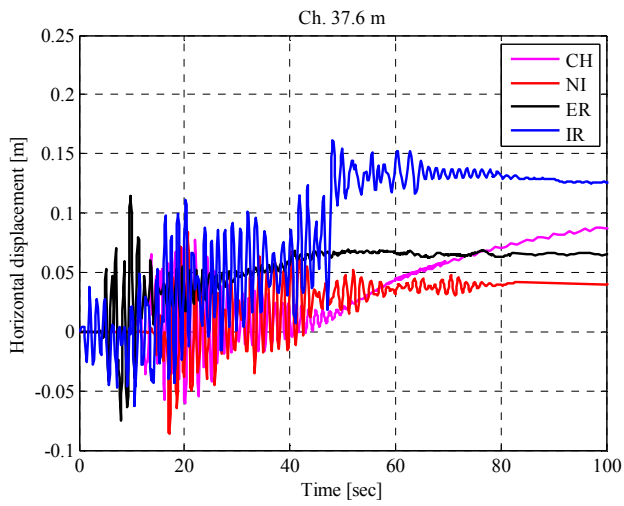
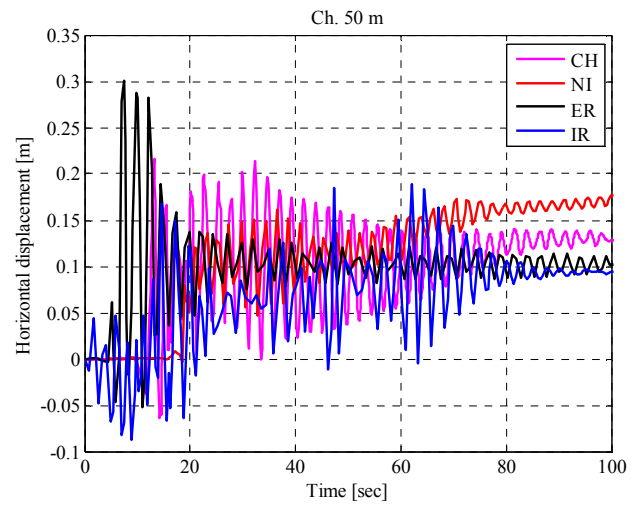


Figure 18. (a) Pseudo-acceleration response spectra of the maximum horizontal component for ground motions reported in Table 6 and elastic spectrum provided by [25]. The ground motions are scaled by the factors reported in the last column of Table 6. (b) Detail of the spectra for the period lying in the range 0–1 s.  $T_{i,38}$  ( $i = 1, \dots, 3$ ) and  $T_{j,50}$  ( $j = 1, \dots, 3, 5$ ) indicate the first three natural periods of the shortened chimney (Table 3) and the first four natural periods of the original chimney (Table 4).



a



b

Figure 19. Top displacement time histories for (a) the shortened and (b) the original chimney.



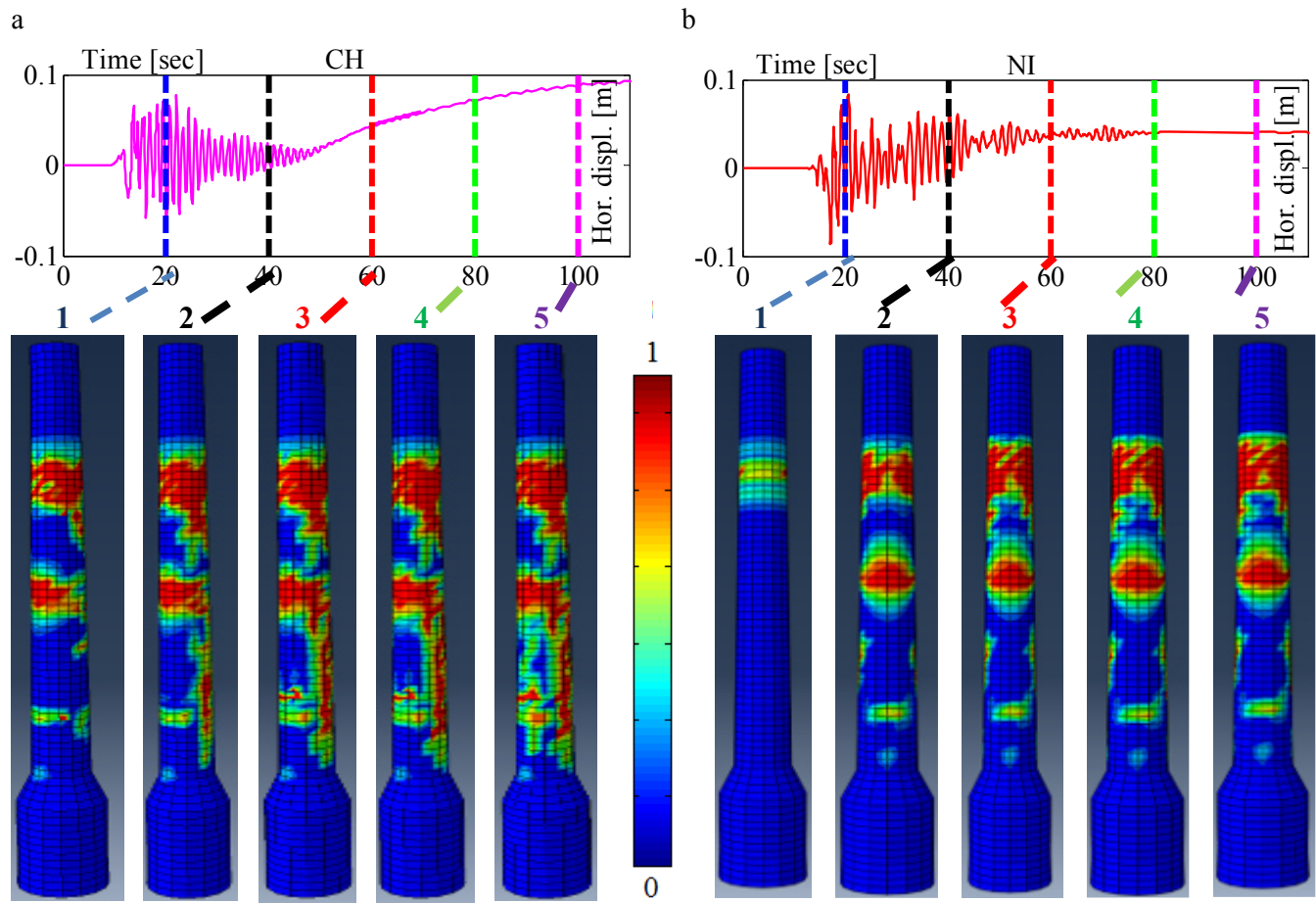


Figure 20. Shortened chimney: damage maps in tension at different time steps for (a) CH and (b) NI ground motions.

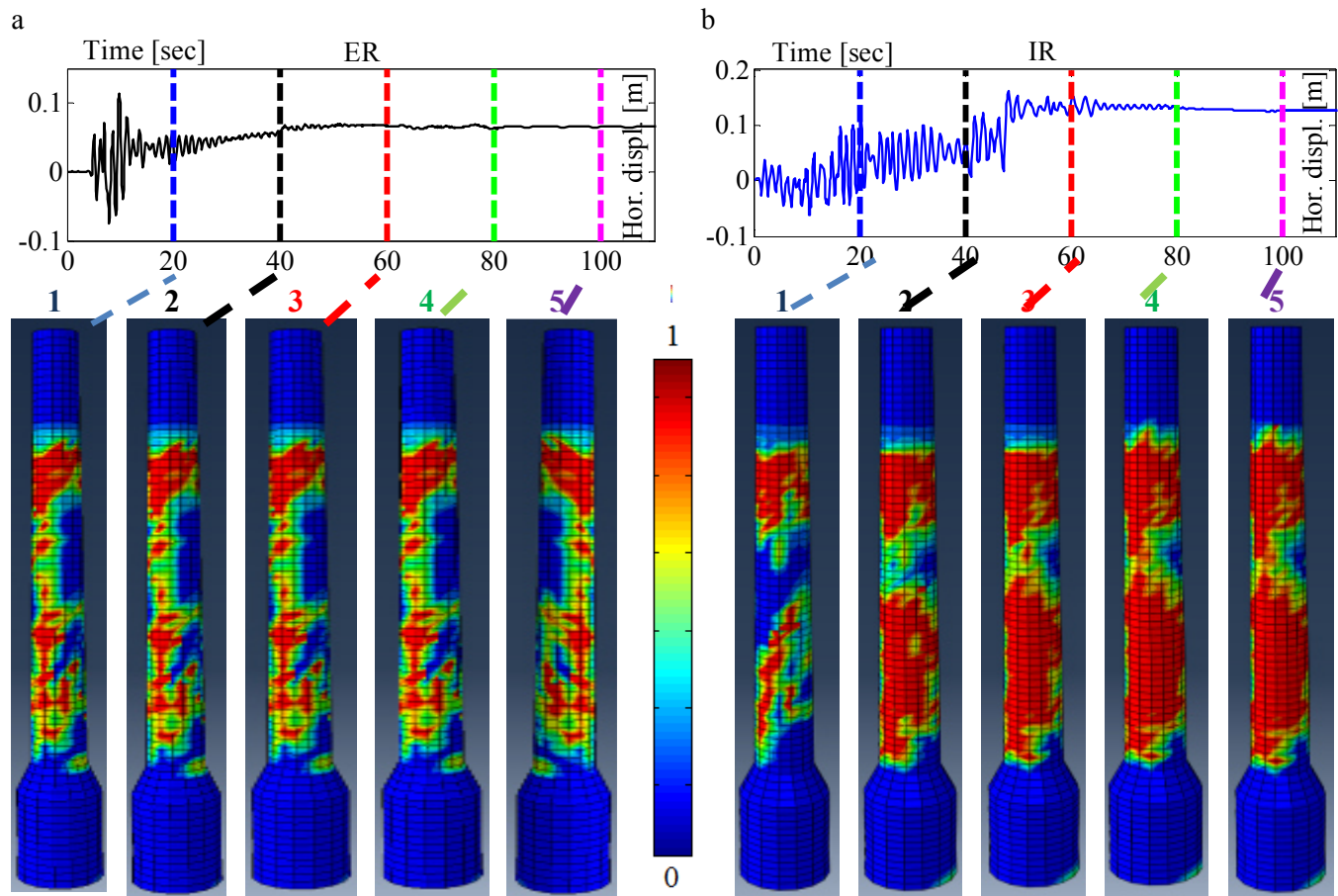


Figure 21. Shortened chimney: damage maps in tension at different time steps for (a) ER and (b) IR ground motions.

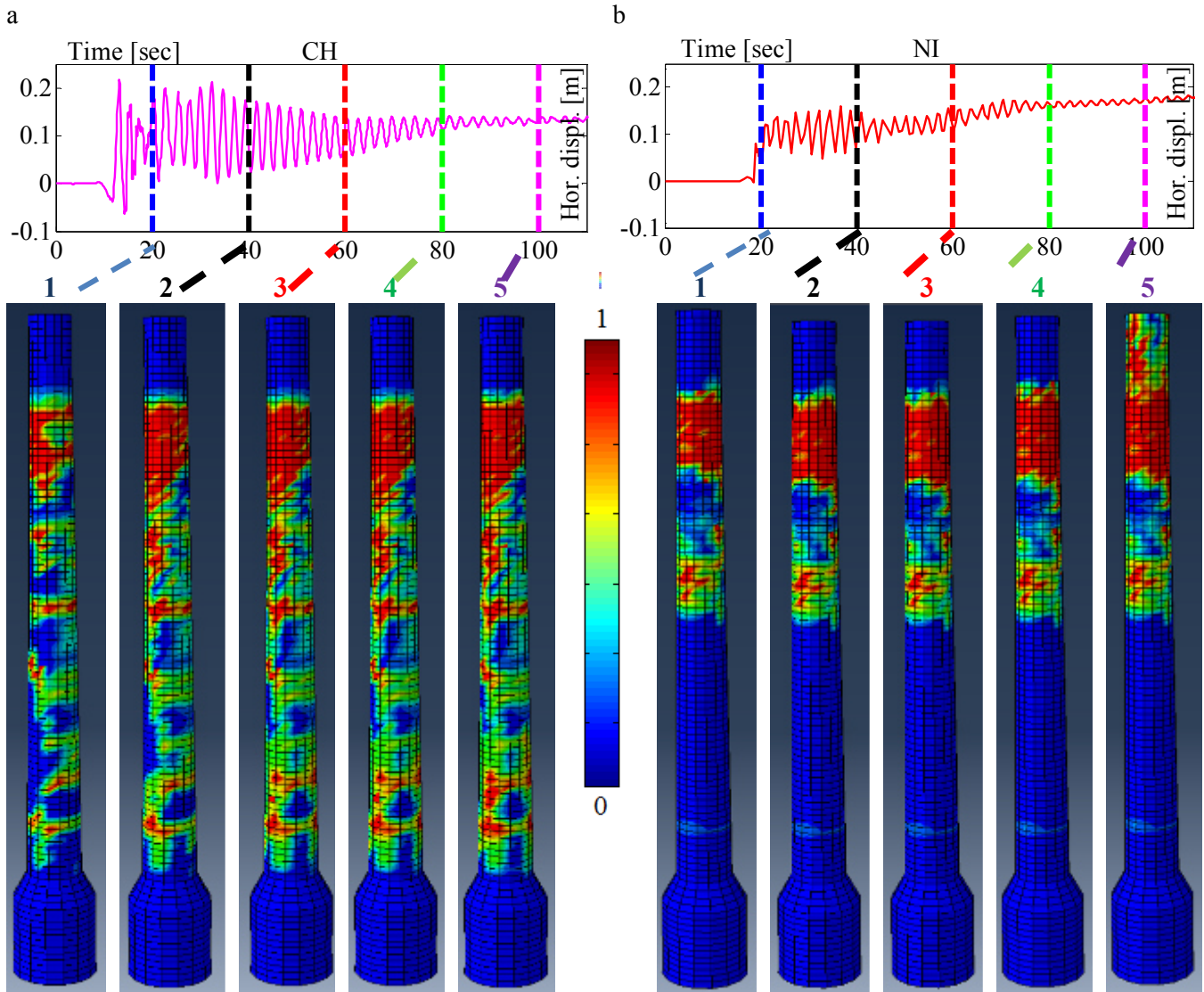


Figure 22. Original chimney: damage maps in tension at different time steps for (a) CH and (b) NI ground motions.

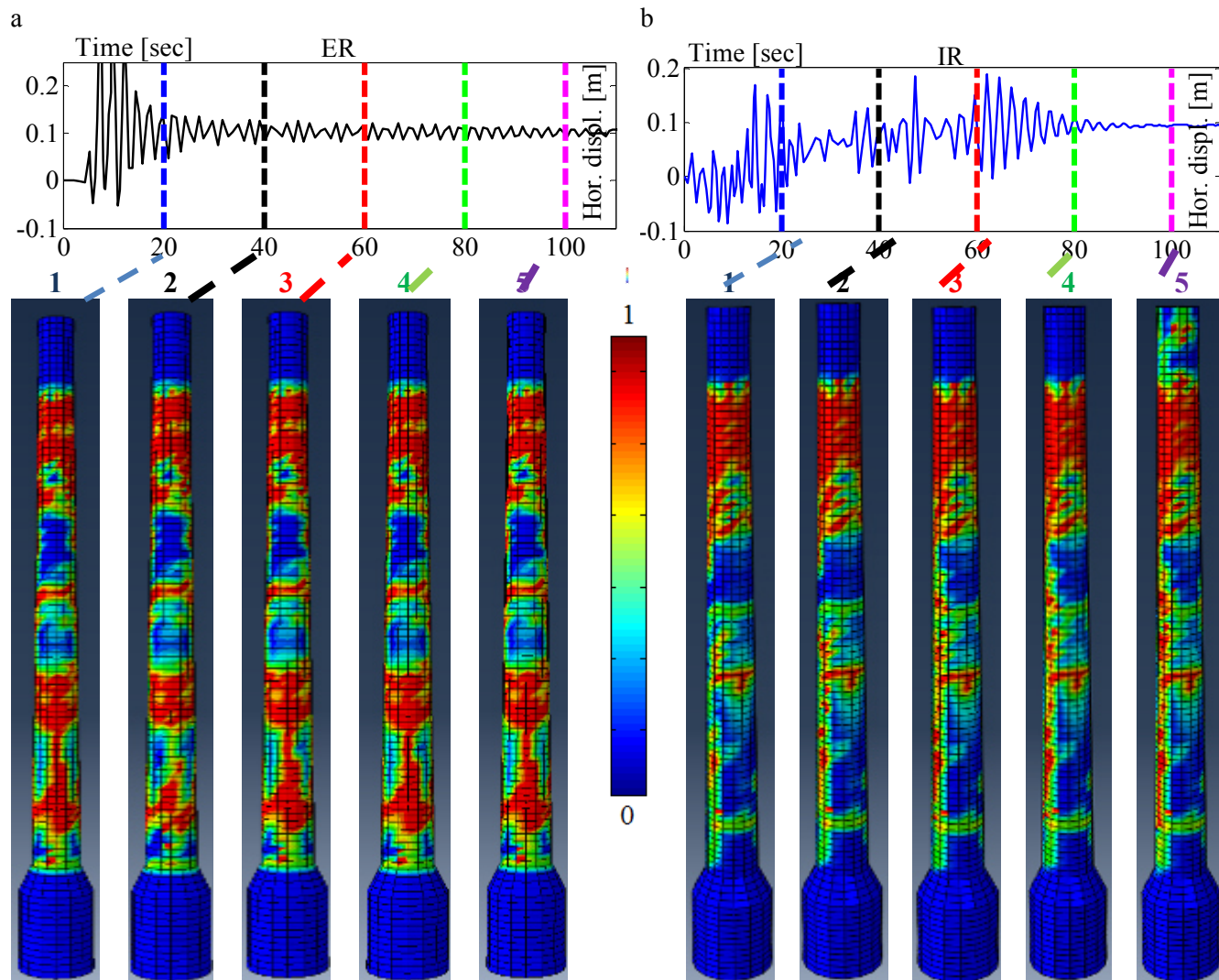


Figure 23. Original chimney: damage maps in tension at different time steps for (a) ER and (b) IR ground motions.